Freezing Drizzle Formation in Stably Stratified Layer Clouds: The Role of Radiative Cooling of Cloud Droplets, Cloud Condensation Nuclei, and Ice Initiation

ROY M. RASMUSSEN

National Center for Atmospheric Research, Boulder, Colorado

ISTVÁN GERESDI

Institute of Geography, University of Pécs, Pecs, Hungary

GREG THOMPSON, KEVIN MANNING, AND ELI KARPLUS

National Center for Atmospheric Research, Boulder, Colorado

(Manuscript received 10 July 2000, in final form 1 March 2001)

ABSTRACT

This study evaluates the role of 1) low cloud condensation nuclei (CCN) conditions and 2) preferred radiative cooling of large cloud drops as compared to small cloud drops, on cloud droplet spectral broadening and subsequent freezing drizzle formation in stably stratified layer clouds. In addition, the sensitivity of freezing drizzle formation to ice initiation is evaluated. The evaluation is performed by simulating cloud formation over a two-dimensional idealized mountain using a detailed microphysical scheme implemented into the National Center for Atmospheric Research–Pennsylvania State University Mesoscale Model version 5. The height and width of the two-dimensional mountain were designed to produce an updraft pattern with extent and magnitude similar to documented freezing drizzle cases. The results of the model simulations were compared to observations and good agreement was found.

The key results of this study are 1) low CCN concentrations lead to rapid formation of freezing drizzle. This occurs due to the broad cloud droplet size distribution formed throughout the cloud in this situation, allowing for rapid broadening of the spectra to the point at which the collision–coalescence process is initiated. 2) Continental clouds can produce freezing drizzle given sufficient depth and time. 3) Radiative cooling of the cloud droplets near cloud top can be effective in broadening an initially continental droplet spectrum toward that of a maritime cloud droplet size distribution. 4) Any mechanism that only broadens the cloud droplet spectra near cloud top, such as radiative cooling, may not act over a sufficiently broad volume of the cloud to produce significant amounts of freezing drizzle. 5) Low ice-crystal concentrations ($<0.08\ L^{-1}$) in the region of freezing drizzle formation is a *necessary* condition for drizzle formation (from both model and observations). 6) Ice nuclei depletion is a *necessary* requirement for the formation of freezing drizzle. 7) The maximum cloud water mixing ratio and threshold amount for the onset of drizzle in stably stratified clouds was shown to depend strongly on the CCN concentration. 8) A key factor controlling the formation of freezing drizzle in stratified clouds is the lifetime of the mesoscale and synoptic conditions and the thickness and length of the cloud.

1. Introduction

Recent studies have shown that freezing drizzle[1] can be a significant safety hazard to aviation due to the potentially dangerous icing it can produce on aircraft (Cooper et al. 1984; Sand et al. 1984; Politovich 1989, 1996). A number of turboprop aircraft accidents have been attributed to the formation of ice on unprotected regions of the wing during these conditions (Marwitz et al. 1997; Pike 1995). Due to their hazardous nature, regions with freezing drizzle are generally avoided by most pilots if possible. In order for them to do this, however, accurate forecasts are required. The quality of freezing drizzle forecasts, however, is limited by a proper physical understanding of the mechanisms by which freezing drizzle forms. Freezing drizzle is generally recognized to form predominantly via an all water process through collision and coalescence of cloud droplets at temperatures below freezing, or the so-called supercooled warm rain process (Ohtake 1963; Kajikawa et al. 1988; Huffman and Norman 1988; Rasmussen et al. 1995; Cober et al. 1996). The main limiting factor in

[1] In this paper we define freezing drizzle to consist of water drops between 50- and 500-μm diameter. Cloud droplets are defined to be water drops less than 50-μm diameter.

Corresponding author address: Roy Rasmussen, NCAR, Box 3000, Boulder, CO 80301.
E-mail: rasmus@ucar.edu

the formation of freezing drizzle is the creation of cloud droplet sizes greater than 40 μm in diameter in order to initiate the collision–coalescence process. Otherwise, the formation of droplets $>$40 μm in diameter through diffusional growth alone is a slow process (Pruppacher and Klett 1997).

The processes causing broadening of cloud droplet size distributions and subsequent drizzle formation in stably stratified layer clouds are currently not well understood. Pobanz et al. (1994) suggested that shear-induced mixing near cloud top may be responsible for this broadening effect. However, more recent studies have found significant amounts of freezing drizzle in clouds with no or minimal shear near their tops (Cober et al. 1996; Isaac et al. 1999; Bernstein 2000). Since many cases of freezing drizzle formation involve frontal situations, it may be that wind shear is associated with the front and not the formation of freezing drizzle. Recent studies (Korelev and Isaac 2000) have suggested that high supersaturations created by isobaric mixing of air parcels in stably stratified environments may be responsible for the broadening of cloud droplet spectra. Again, a mixing process is required for this mechanism, which is not always observed with clouds associated with freezing drizzle.

Observational studies by Murakami et al. (1992), Rasmussen et al. (1995), and Cober et al. (1996) have suggested that low concentrations of cloud condensation nuclei (CCN) may be responsible for the rapid growth of cloud droplets to sizes large enough to initiate the collision–coalescence process in these types of stably stratified clouds. Another possible mechanism for cloud droplet spectral broadening is radiative cooling of the individual cloud droplets (Roach 1976). This effect has mainly been studied in the context of fogs and stratocumulus clouds (Roach 1976; Caughey and Kitchen 1984; Chen and Cotton 1987; Austin et al. 1995; Harrington et al. 2000). In these cloud types, radiative cooling of the individual drops was shown to broaden the spectra faster than pure diffusional growth. However, in stratocumulus clouds, the effect on drizzle formation was relatively small due to the short residence time of air parcels near cloud top (Harrington et al. 2000).

In this paper we evaluate the role of 1) low CCN conditions, and 2) preferred radiative cooling of large cloud drops as compared to small cloud drops, on cloud droplet spectral broadening and subsequent freezing drizzle formation in stably stratified layer clouds. In addition, we also evaluate the sensitivity of freezing drizzle formation to the concentration of ice forming nuclei (IFN). The current simulations do not address enhanced freezing drizzle formation due to mixing processes as proposed by Pobanz et al. (1994), Korelev and Isaac (2000), and Cooper (1989) nor enhanced drizzle formation due to curvature and salinity effects as discussed by Celik and Marwitz (1999) and Korelev (1995) or the possible role of giant nuclei (Feingold et al. 1999). These processes may further enhance the formation of freezing drizzle in the type of clouds studies herein and will be addressed in future studies.

The current evaluation is performed by simulating cloud formation over a two-dimensional idealized mountain using a detailed microphysical scheme implemented into the National Center for Atmospheric Research–Pennsylvania State University (NCAR–PSU) Mesoscale Model version 5 (MM5). The height and width of the two-dimensional mountain were designed to produce an updraft pattern with extent and magnitude similar to documented freezing drizzle cases (Rasmussen et al. 1995; Cober et al. 1996; Bernstein et al. 1997; Bernstein 2000).

The detailed microphysical scheme is described in section 2, and its implementation into the NCAR–PSU MM5 is discussed in section 3. Section 4 provides an analysis of the results. Section 5 compares the results to observations of the freezing drizzle formation in the 1990 Valentine's Day freezing drizzle event in Colorado (Rasmussen et al. 1995) and to other freezing drizzle observations made in North America (Cober et al. 1996; Stuart and Isaac 1999; Bernstein 2000). Conclusions are given in section 6.

2. Description of the detailed microphysical scheme

A detailed microphysical scheme was developed to simulate the formation of freezing drizzle and various ice species in stably stratified clouds based on the model of Geresdi (1998). A key improvement over the previous Geresdi (1998) model is the implementation of the moment-conserving technique (Reisin et al. 1996) for calculation of the time evolution of the hydrometeor size distributions (see appendix for details of the model). The moment-conserving technique has been demonstrated to accurately model the evolution of hydrometeor distributions by Tzivion et al. (1987, 1999). The main achievement of the moment conserving technique is the prevention of artificial broadening of the hydrometeor size distribution by numerical diffusion. In addition, the moment-conserving technique conserves mass and number concentration independent of time step and bin size.

The modified model simulates five different types of hydrometeors: water drops, pristine ice crystals, rimed ice crystals, snowflake aggregates, and graupel (see appendix section a for details on the shape, density, axis ratio, and terminal velocities assumed for each hydrometeor type). Thirty-six size bins are used to describe the evolution of the size distribution for each of these five hydrometeor types. Bins are delineated by edges with the next largest edge having a mass double that of the previous edge. The mass range for all five hydrometeor types is 1.5979×10^{-14}–0.001098 kg (1.56 μm–6.4 mm for water drops), with $m_{k+1} = 2m_k$ (where m is mass and k the bin index). Cloud droplets are initialized based on specified equations for CCN cumulative concentration [N_{CCN} (cm^{-3})] as a function of supersaturation, S (%)

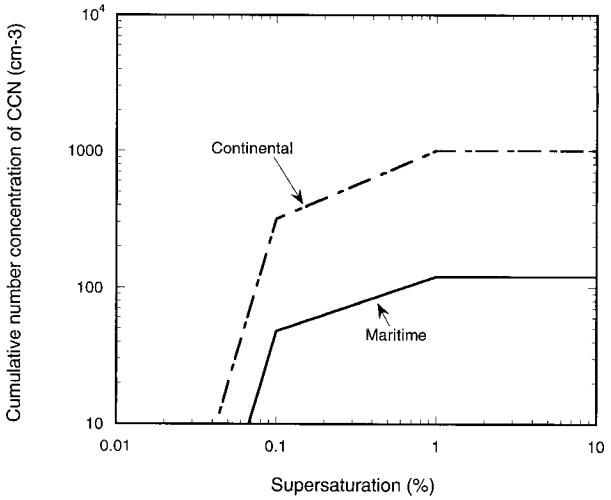

FIG. 1. Maritime and continental CCN cumulative number concentration (cm^{-3}) as a function of supersaturation S (%) over a flat water surface. See text for details of the functions.

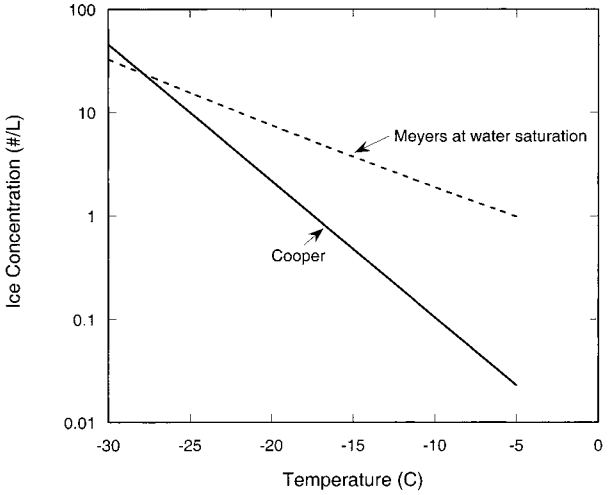

FIG. 2. Ice initiation scheme for deposition and condensation ice nucleation as a function of temperature for the Meyers et al. (1992) and Cooper (1986) schemes. See text for details of the functions.

over a flat water surface. In this study we use CCN spectra typical of maritime and continental air masses (Fig. 1). The continental CCN concentration is given by

$$N_{\mathrm{CCN}} = \begin{cases} 3.16 \times 10^6 S^4 & \text{if } S < 0.1 \\ 1000 S^{0.5} & \text{if } 0.1 < S < 1.0 \\ 1000 & \text{if } S > 1.0 \end{cases} \quad (1)$$

and the maritime distribution by

$$N_{\mathrm{CCN}} = \begin{cases} 4.78 \times 10^5 S^4 & \text{if } S < 0.1 \\ 120 S^{0.4} & \text{if } 0.1 < S < 1.0 \\ 120 & \text{if } S > 1.0. \end{cases} \quad (2)$$

The continental distribution was developed from CCN observations near Colorado, and the maritime distributions from CCN measurements near Hawaii. Both measurements were made by Jim Hudson of Desert Research Institute (1999, personal communication) with his CCN instrument. CCN particles are assumed to be monodisperse and drops just formed on them are put into the first water droplet size category. The time step used to give the concentration of the newly formed drops on CCN and to calculate the diffusional growth was reduced to 1 s, while for the other processes a 10-s time step was used.

Ice is initiated in the pristine ice category using equations that produce ice by deposition, condensation-freezing, immersion, and contact nucleation (see appendix section d for details on contact nucleation). Two types of equations are used for deposition and condensation freezing: an equation by Meyers et al. (1992) based on laboratory measurements of natural ice nuclei using a continuous flow diffusion chamber, and a fit to in situ ice crystal measurements by Cooper (1986). Individual simulations use one or the other of these equations. The Meyers equation is given by

$$N_{i,\mathrm{Meyers}} = \exp(-0.639 + 0.1296 S_i) \quad (3)$$

and the Cooper equation by

$$N_{i,\mathrm{Cooper}} = 0.005 \exp[0.304(T_o - T)], \quad (4)$$

where S_i is the supersaturation(%) with respect to ice, N_i the number concentration in # L^{-1}, $T_o = 273.15$ K, and T is the ambient temperature in K. A plot of these two relationships is shown in Fig. 2. In both cases, pristine ice crystals are initiated only if the temperature is less than -5°C and water saturation is reached. At temperatures <-27°C both schemes are set to the ice concentration value at -27°C to prevent the formation of unrealistically high numbers of pristine ice crystals at colder temperatures.

In bulk microphysical parameterizations, only one or two variables are typically available to describe the size distribution. In most cases the mixing ratio is predicted and the shape and parameters of the size distribution are assumed. The use of 36 bins in the current detailed microphysical model allows the size distribution of the five hydrometeor types to evolve naturally without having to specify the shape of the size distribution.

The following growth/evaporation/melting processes are simulated in the detailed model:

1) Diffusional growth of water drops, pristine ice, and rimed ice (see appendix section b for details).
2) Freezing of supercooled drops. If the diameters of the drops are <50 μm, pristine ice crystals are formed. Larger drops become graupel.
3) Melting of graupel.
4) Collision and coalescence of water droplets.
5) Pristine ice crystal and water drop collisions to form rimed ice. If the mass of the water drop is greater than the pristine ice crystal, then graupel forms.
6) Rimed ice crystal and water drop collisions result in the growth of rimed ice. If the mass of the water

drop is greater than the rimed ice crystal, graupel forms.
7) Self collisions between pristine ice crystals and rimed ice crystals form snowflake aggregates.
8) Riming of aggregates results in graupel.
9) Riming of graupel increases the mass of the graupel.

In addition to the continuity equations for the hydrometeors, continuity equations are also included for CCN and activated ice nuclei (IN). These equations allow for the depletion of CCN and IN as well as sources and sinks.

Ice nuclei are activated whenever pristine ice crystals are formed. The sources of activated ice nuclei are given by the Meyers or Cooper scheme for deposition and condensation freezing nucleation or by contact ice nucleation (as given in the appendix). For condensational freezing and depositional nucleation, the new crystals are assumed to be monodisperse with a mass of 0.5 ($m_2 + m_3$) and put into the second bin. The increase in number concentration and mixing ratio of the pristine ice crystals due to deposition or condensation freezing during time step Δt is given by

$$\Delta N_{\text{ic}} = \Delta N_{\text{id}} = N_{\text{id}}(t) - N_{\text{id}}^1 \quad \text{and}$$

$$\Delta M_{\text{ic}} = \Delta N_{\text{id}} \cdot 0.5(m_1 + m_2),$$

where N_{id}^1 is the concentration of activated ice nuclei including advection and diffusion at a grid point and $N_{\text{id}}(t)$ is the maximum concentration of ice nuclei that could be activated at a grid point at time t from Eq. (3) or (4). New ice crystals can form if $\Delta N_{\text{id}} > 0$. Models without ice nuclei depletion will overestimate ice crystal concentrations when ice crystals sediment or collide with each other and form aggregates.

A new aspect of the model is the inclusion of radiative cooling effects of the drops when calculating water droplet diffusional growth. The equations used for this calculation are

$$\frac{dm}{dt} = 4\pi r D_v[\rho_\infty(T_\infty) - \rho_{s,w}(T_s)]f_v, \tag{5}$$

$$L_v\frac{dm}{dt} + 4\pi r^2 Q_r = 4\pi r k_a(T_s - T_\infty)f_h, \tag{6}$$

where Q_r is the net radiative heat loss per unit surface area of water drops (this term is taken into consideration only at the top of the cloud, in the interior of the cloud the net radiative heat loss is zero). The formulation of Q_r for drizzle clouds is based on the observation that these cloud types are stratiform with a dry layer aloft. An appropriate formulation for describing cloud top cooling for this type of cloud is given by Roach (1976):

$$Q_r = -0.15 Q_a \sigma T^4, \tag{7}$$

where $Q_a(r) = Q_{\max}[1 - \exp(-\beta r)]$ is the mean absorption efficiency averaged over wavelength, and σ is the constant in the Stefan–Boltzmann radiation law (5.67×10^{-8} W m^{-2} K^{-4}), $Q_{\max} = 1.18$, and $\beta = 0.28$ μm^{-1}. Only longwave cooling is considered in the current treatment in order to maximize the potential effect of cooling on broadening the cloud droplet spectra. Here f_v and f_h are the ventilation coefficients for diffusion and heat conduction (Pruppacher and Klett 1997). The gas kinetic effect is also taken into consideration (which decreases the growth rate of the small droplets). The resulting growth rate of a drop including radiative effects is then given by

$$\frac{dm}{dt} = \frac{4\pi r(q_v - q_{s,w})f_v - \dfrac{q_{s,w}}{k_a T}\left(\dfrac{L_v}{R_v T} - 1\right)4\pi r^2 Q_r}{q_{s,w}\left[\dfrac{L_v}{k_a T}\left(\dfrac{L_v}{R_v T} - 1\right) + \dfrac{R_v T}{D_v e_{s,w}(T)F_\alpha}\right]}, \tag{8}$$

where F_α is given in Pruppacher and Klett (1997). Section c of the appendix presents a derivation of the supersaturation excess over ice and over water modified by the effect of radiative cooling of drops.

3. Approach

The detailed study by Rasmussen et al. (1995) describes a freezing drizzle case that formed in association with the uplift of air over an artic front in Colorado. The magnitude of the uplift was documented to be on the order of 6–10 cm s^{-1} based on isentropic analysis and Velocity Azimuth Display (VAD) analysis from radar. Freezing drizzle formed in the stably stratified upper portion of the cloud in association with liquid water contents up to 0.35 g m^{-3}. In the region of drizzle formation, the cloud-top temperature was -10°C and low ice-crystal concentrations were present. Cober et al. (1996) documented a case with supercooled drizzle over the Atlantic Ocean in which the cloud-top temperature was -12°C, vertical velocity between 5 and 7 cm s^{-1}, maximum liquid water content 0.2 gm^{-3}, and ice-crystal concentration 0.08 L^{-1}. The formation of drizzle in regions of weak mesoscale ascent, warm cloud tops, low ice-crystal concentrations, and stably stratified conditions has been documented by a number of other studies as well (Murakami et al. 1992; Bernstein et al. 1998; Bernstein 2000). The climatological study of Bernstein et al. (1998) identified three main regions for freezing drizzle formation in association with synoptic-scale extratropical cyclones: 1) ahead of a warm front in the overrunning region, 2) near a low pressure center, and 3) at the leading edge and toward the rear of arctic and cold fronts. All of these regions have relatively warm cloud tops (typically -12°C and greater), mesoscale uplift on the order of 5–20 cm s^{-1}, and stably stratified conditions.

In order to understand the processes leading to freezing drizzle in these types of stably stratified clouds, the detailed microphysical model described in section 2 was implemented into a two-dimensional version of the

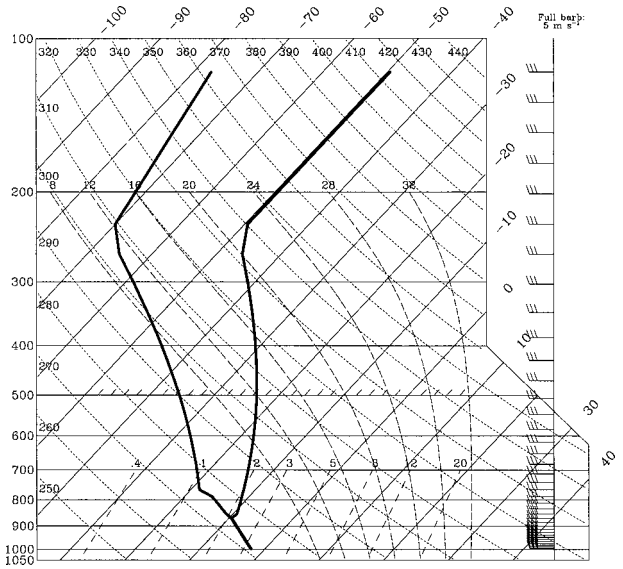

FIG. 3. Sounding used to initialize the freezing drizzle cloud in the model. Wind barbs plotted at every σ level of the model. Full barb represents 5 m s^{-1}.

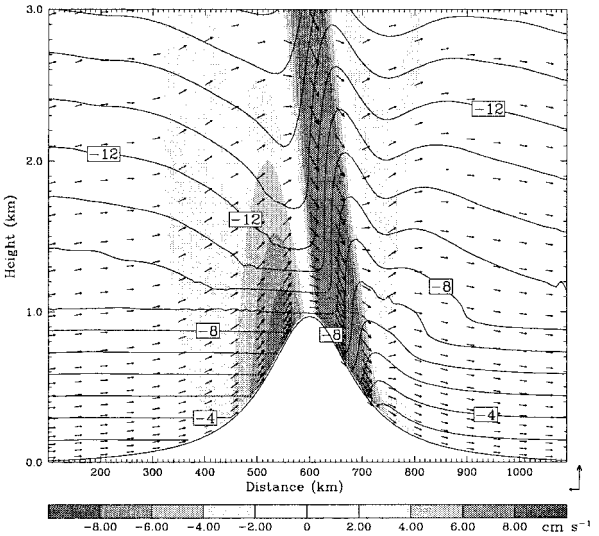

FIG. 4. Vertical motion (cm s^{-1}) field (gray shades), temperature contours (°C), and wind vectors from simulation 6 at 2 h. Gray scale vertical motion values in cm s^{-1} indicated in the legend below the figure. Shading indicates upward (downward) velocity depending on whether wind vectors indicate upward (downward) motion. The horizontal component of the wind vector is proportional to the horizontal component of wind in m s^{-1} and the vertical component of the wind vector is proportional to the vertical velocity in cm s^{-1}. The wind vector scale is shown at the lower-right-hand corner of the plot, with the length of the horizontal vector = 20.3 m s^{-1} and the vertical vector = 17.3 cm s^{-1}.

NCAR–PSU MM5 model (Dudhia 1993). The above-described synoptic conditions were simulated by using a two-dimensional bell-shaped mountain to force a mesoscale uplift of 5–10 cm s^{-1} over a distance of approximately 100 km. This was achieved using the sounding shown in Fig. 3. This sounding has an entirely subfreezing moist adiabatic saturated layer from the surface to cloud top at −10°C. Above cloud top, the sounding dries out and becomes more stable. While the cloud layer is neutral and thus not absolutely stable, it allows for the simulation of airflow typically observed during isentropic lift over a front through the use of a simple two-dimensional barrier (Fig. 4). If the cloud layer in this sounding were stable, flow blocking would occur at low levels, and the resulting airflow would be unrepresentative of airflow over a frontal surface.

The wind speed impacting the barrier is 15 m s^{-1}, resulting in a vertical motion field as shown in Fig. 4, with vertical motion on the order of 5–10 cm s^{-1} on the upstream 100 km of the barrier and downward motion to the lee of the barrier. The formation of freezing drizzle is simulated in the vertical motion field on the upstream side of the mountain. The bell-shaped mountain has a height of 1 km and a half-width of 100 km.

Table 1 describes the simulations performed using the sounding discussed above. As shown, simulations were

TABLE 1. Summary of 2D simulations using the detailed microphysical model.

	Ice scheme	CCN type	Mixed phase or only liquid	Radiation cooling of drops on/off	Simulation time (hours)
Simulation 1	None	Continental	Liquid only	Off	6
Simulation 2	None	Continental	Liquid only	On	6
Simulation 3	Meyers	Continental	Mixed phase	Off	3
Simulation 4	Meyers	Continental	Mixed phase	On	3
Simulation 5	Meyers	Maritime	Mixed phase	On	3
Simulation 6	Cooper	Maritime	Mixed phase	On	3
Simulation 7	None	Maritime	Liquid only	Off	6
Simulation 8	None	Maritime	Liquid only	On	6
Simulation 9	Cooper	Maritime	Mixed phase	Off	3
Simulation 10	Cooper with no ice nuclei depletion	Maritime	Mixed phase	On	3
Simulation 11	None	Continental	Liquid only	On with two vertical grid points	6
Simulation 12	Cooper	Continental	Mixed phase	On	6

performed in which the ice phase was turned on and off for both continental and maritime CCN distributions, radiative cooling on and off, ice nuclei depletion on and off, and with the Meyers and Cooper ice schemes.

The time step used for all the simulations was 10 s and the horizontal grid spacing 10 km with a 1200-km horizontal domain length. Tests were performed with shorter time steps and horizontal grid spacings and the results were found not to change significantly. The top of the domain was 100 mb, and 39 vertical grid levels in σ coordinates were used. The effective vertical grid spacing in the lower region of the cloud was ~50 m and in the upper cloud region ~150 m. The vertical location of the wind barbs in Fig. 3 is given at each of the σ levels.

4. Results

a. Discussion of a typical case: Mixed phase simulation with radiative cooling of drops on, Cooper ice initiation, and a maritime CCN distribution (simulation 6)

The lifting of moist air over the two-dimensional barrier results in the formation of cloud water on the upstream side of the barrier, with the maximum cloud water (0.36 g kg^{-1}) after 3 h of simulation time located 80 km upstream of the mountain peak and within 1 km of the surface (Fig. 5a). Note that the cloud water increases from west to east at a rate proportional to the slope of the topography. Drizzle forms once the cloud water content exceeds 0.35 g kg^{-1} (Fig. 5b). The threshold of 0.35 g kg^{-1} is consistent with observations of the onset of freezing drizzle from the Winter Icing and Storm Project (WISP; Rasmussen et al. 1992) case study by Rasmussen et al. (1995), which had low cloud droplet concentrations similar to that found in the current maritime drizzle simulation.

Pristine ice crystals formed at cloud top where the coldest temperatures are encountered (Fig. 5c). Once these crystals fall into the cloud water region they rapidly convert to rimed crystals (Fig. 5d). A small number of the rimed crystals collide with each other to form aggregates (Fig. 5e), and some of the rimed crystals and aggregates collide with larger drops to form graupel particles (Fig. 5f). Both the aggregates and graupel particles are located near the top of the barrier within the region of cloud liquid water, drizzle, and rimed crystals and have mixing ratios 2–4 orders of magnitude less than the rimed ice crystals.

b. Effect of maritime versus continental CCN on freezing drizzle formation

We consider in this section the all-water simulations 1 and 7 with no cloud droplet cooling due to radiation in order to examine the effect of continental versus maritime CCN on the formation of freezing drizzle. Freezing drizzle appears in the maritime simulation after 1 h of simulation time (Fig. 6). The cloud water mixing ratio reaches a domain maximum value of 0.36 g kg^{-1} at this time. In contrast, the onset of drizzle in the continental CCN case occurs after 3 h of simulation time, at which point the cloud water mixing ratio has reached a value of 0.75 g kg^{-1}, double the maximum value in the maritime case (Fig. 6).

The evolution in time and space of the droplet spectrum for the maritime case is shown in Fig. 7 at 250 m above the terrain every 0.5 h. Droplets with diameters greater than 40 μm first appear in the maritime simulation as a result of condensational growth after 30 min of simulation time. The onset of collision–coalescence is evident between 60 and 90 min near 500 km by the rapid increase in droplet diameters at that location and time (evident by the ''bump'' in the contour plot of concentration as a function of droplet diameter in Fig. 7). Once collision–coalescence starts, freezing drizzle forms rapidly (within 30 min).

The growth of the droplet spectra to larger sizes as an air parcel advects toward the mountain is indicated by the upward tilt of the concentration contours toward the right (in the direction of flow). In the maritime case (Fig. 7), the upward tilt is larger than in the continental case (Fig. 8), indicating that the maritime droplet size spectra evolve to larger sizes more rapidly than the continental droplet size spectra.

A droplet diameter of 40 μm is first exceeded in the continental case (Fig. 8) after 120 min of simulation time, four times longer in time than the maritime case. As a result, significant drizzle does not form in the continental CCN case until 4 h after the start of the simulation as compared to 1.5 h in the maritime case.

The evolution of the size distribution for the maritime case following a parcel 250 m AGL is shown in Fig. 9a. This parcel is located 135 km upstream of the mountain top at $t = 0.5$ h. The spectrum at the initial location starts off relatively broad with small numbers of droplets (~50 cm^{-3}). As the air parcel moves closer to the mountain peak, the spectrum broadens and the overall spectrum shifts to larger diameters. By 2.0 h the spectrum has significantly broadened and drizzle drops have formed.

→

FIG. 5. Two-dimensional vertical cross sections from simulation 6 at 3 h: (a) cloud liquid water (g kg^{-1}), (b) rainwater mixing ratio (g kg^{-1}), (c) pristine ice mixing ratio (g kg^{-1}), (d) rimed ice crystal mixing ratio (g kg^{-1}), (e) snow aggregate mixing ratio (g kg^{-1}), and (f) graupel particle mixing ratio (g kg^{-1}). Grayscale values and units indicated in the legend on the bottom of each panel.

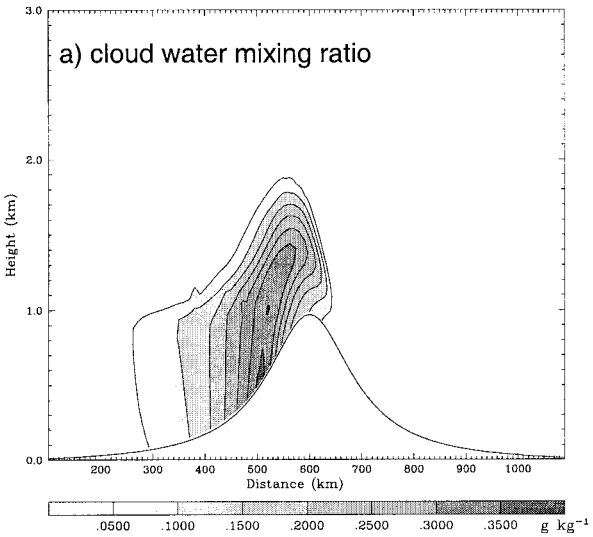

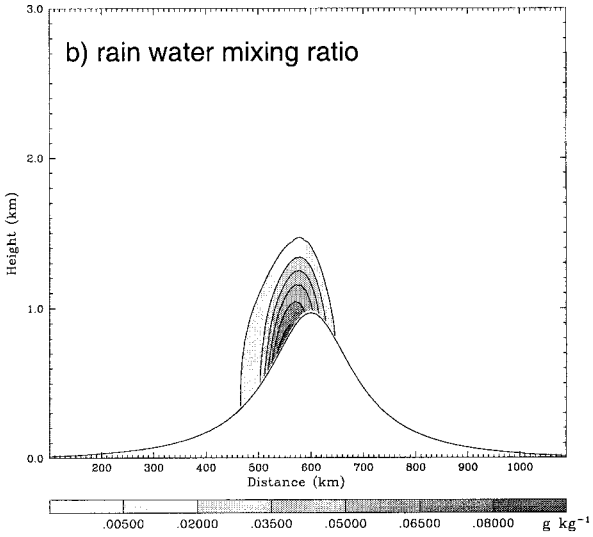

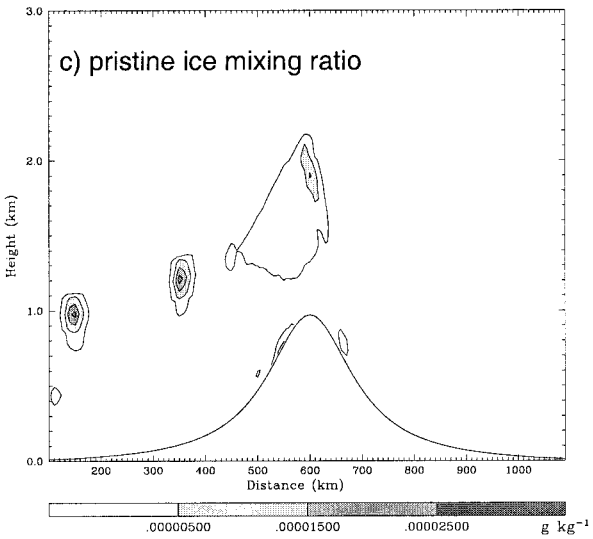

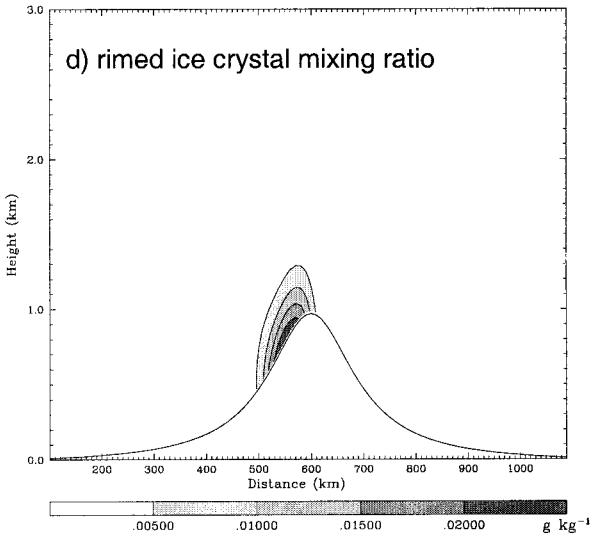

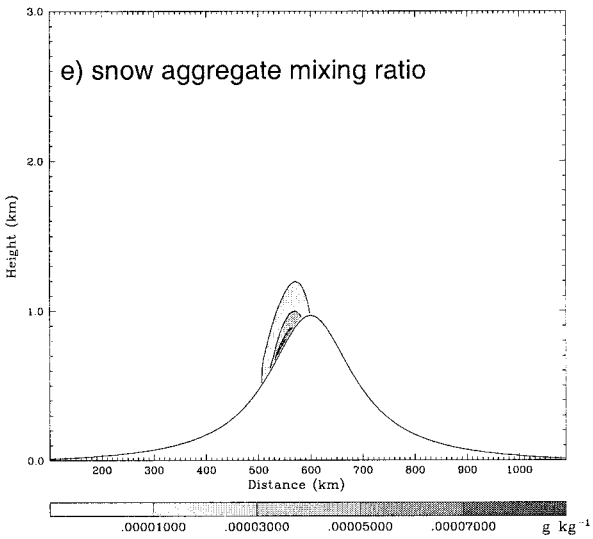

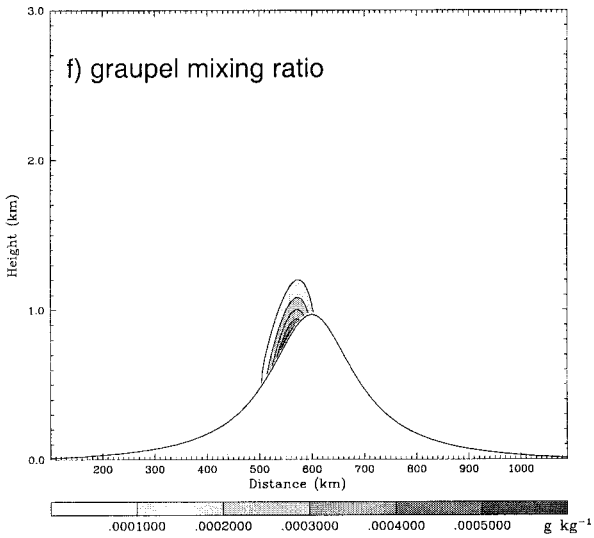

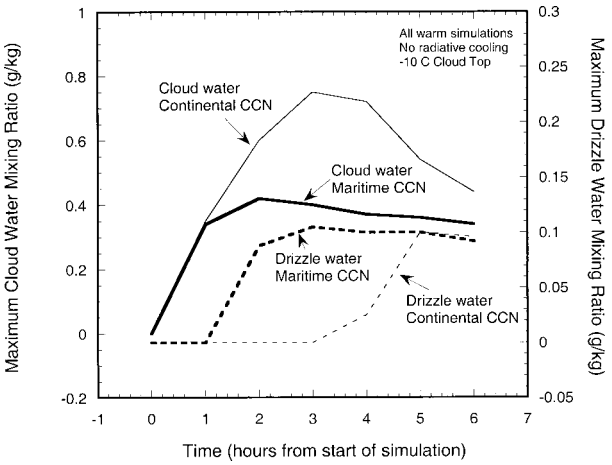

FIG. 6. Time series of the maximum drizzle water mixing ratio (g kg^{-1}) and cloud water mixing ratio (g kg^{-1}) for simulation 7 (all warm maritime case) and simulation 1 (all warm continental case).

In the continental case, the trajectory ending up at mountain top after 6 h (Fig. 9b) starts 300 km upstream of the mountain at $t = 0.5$ h. This parcel trajectory will experience a slightly different updraft magnitude with time than the previous trajectory. The initial size distribution ($t = 0.5$ h) for this trajectory (Fig. 9b) has a narrower size distribution with high number concentration ($\sim$300 cm^{-3}) that shifts to larger diameters as the parcel approaches the mountain, but does not broaden significantly. By 4.5 h the spectrum has broadened and drizzle size droplets have formed. Thus, the onset of drizzle for the continental case is due to the spectrum moving to larger sizes without significant spectral broadening until sufficient numbers of 40-μm droplets have developed (after 3 h in Fig. 9b). The slightly different updraft magnitude experienced by this parcel should not affect these results significantly, since they mainly rely on the cloud water content, which was shown to be significantly larger in the continental case than in the maritime case.

A plot of water drop concentration as a function of time and height at $x = 550$ km is shown in Fig. 10a for the maritime case and in Fig. 10b for the continental case. The evolution with time of the drop size distribution shows the initial formation of 50- and 200-μm drops occurring at nearly the same time at all altitudes, except for the height just below cloud top (820 m). In the maritime case the spectral broadening to 200 μm occurs between 1.6 and 2.1 h, while in the continental case it occurs between 3.8 and 4.5 h. The relatively small time differences in the formation of 200-μm drops at different levels is due to the fallout of the drizzle droplets. The nearly simultaneous spectral broadening at all altitudes reflects the fact that each air parcel for a given CCN distribution has a nearly similar cloud droplet distribution initially and is subject to similar magnitudes of lifting. Thus, the formation of drizzle-sized drops is expected to occur at nearly the same time at all altitudes in the cloud for a given CCN distribution. This figure also shows what a vertically pointing remote sensing device might observe as a function of height and time above an area of active freezing drizzle formation.

The maximum diameter of the drizzle drops was 300 μm in both the maritime and continental cases. Maximum drizzle water contents were also near 0.1 g kg^{-1} in both cases (Fig. 6). Both the maximum size and mixing ratio predicted by the model agree well with airborne and surface observations of freezing drizzle (Politovich 1989; Rasmussen et al. 1995; Cober et al. 1996; Bernstein 2000). Maximum cloud water content in the maritime simulation reached 0.44 g kg^{-1}, nearly a factor of two less than the continental simulations, reflecting the more efficient conversion of cloud water to drizzle water in the maritime case.

These model results show that drizzle can form in moderate mesoscale updrafts in both maritime and continental CCN conditions. However, the maritime case formed drizzle after only 90 min, while the continental case took over 4 h. Thus, low CCN conditions are clearly more favorable to freezing drizzle formation than high CCN conditions. Freezing drizzle formation by low CCN concentrations was proposed by Murakami et al. (1992) to explain freezing drizzle formation in warm frontal situations, by Rasmussen et al. (1995) to explain freezing drizzle formation in arctic fronts, and by Cober et al. (1996) to explain freezing drizzle formation in maritime clouds off Nova Scotia.

The study by Stuart and Isaac (1999) using 30 yr of surface data from Canada showed that freezing drizzle frequently occurs near the Atlantic Ocean. For instance, they documented that freezing drizzle frequently occurred during winter months in the Maritime Provinces and eastern Newfoundland, all of which are located near the Atlantic Ocean. St. John's, in eastern New Foundland, for instance, has over 100 h of freezing drizzle annually, the highest frequency of drizzle occurrence in North America (and possibly the world). The air masses in these regions typically have low CCN concentrations due to their maritime origin.

Analysis of data collected during the NASA/Glenn freezing drizzle field programs near Cleveland also showed that freezing drizzle most often forms in clean air masses. It was observed that air masses with trajectories over the Great Lakes were more likely to form freezing drizzle than air masses with continental sources (Bernstein 2000).

c. Effect of radiative cooling of drops near cloud top on freezing drizzle formation

In order to examine the effects of radiative cooling of cloud drops near cloud top on freezing drizzle formation, we compare simulations 1 and 2 for the continental CCN distribution and simulations 7 and 8 for the maritime CCN distribution. We also consider sim-

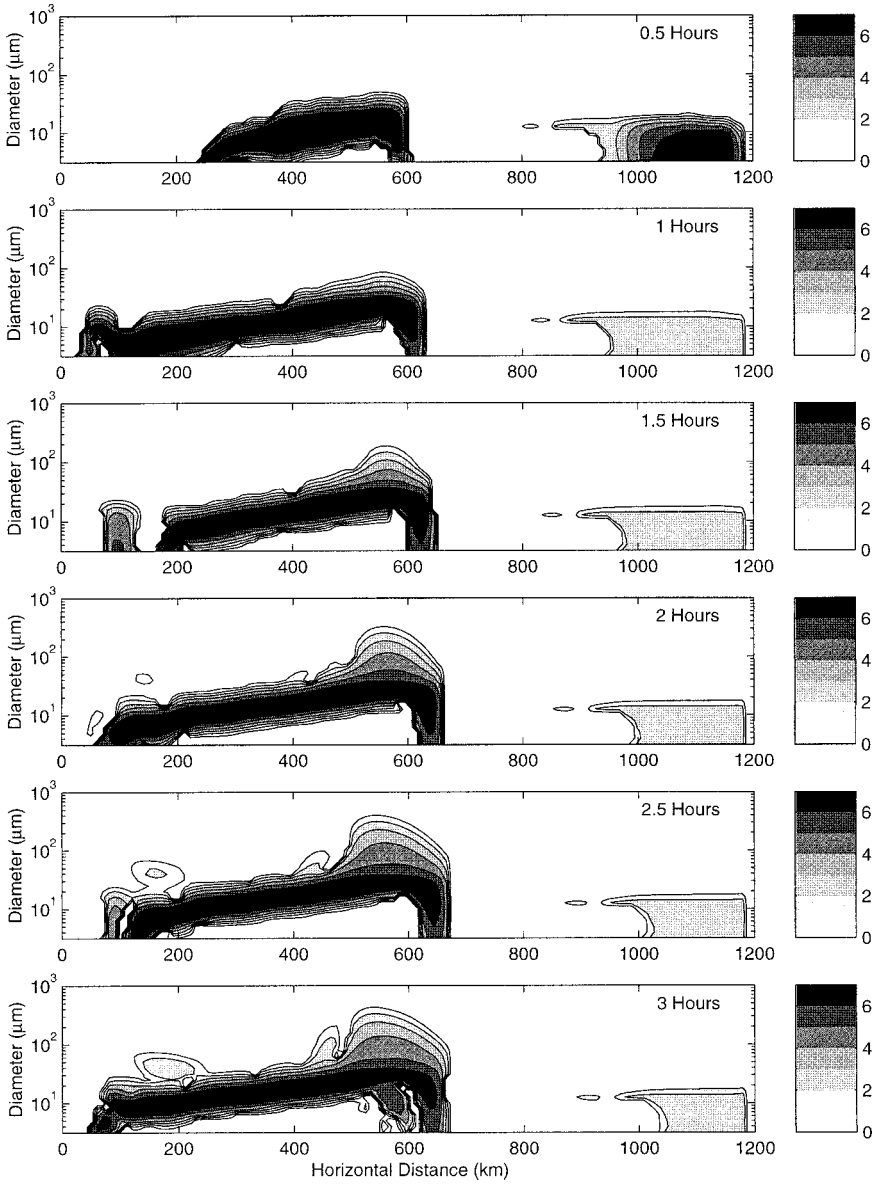

FIG. 7. Logarithmic gray shade contours of droplet number density [# kg^{-1} (d logr^{-1})] using the gray scale at the right as a function of water droplet diameter (vertical axis) and distance (km) 250 m above the ground level for simulation 7 (all warm maritime simulation) at, from top to bottom: 0.5 h, 1.0 h, 1.5 h, 2.0 h, 2.5 h, and 3.0 h.

ulation 11 in which the depth over which radiative cooling is applied near cloud top is doubled. All of these simulations consider liquid phase only.

A 1D detailed simulation of the radiative cooling at cloud top using the vertical profile of cloud water found in the current simulations revealed a maximum cooling rate of -30 K day^{-1} confined to the upper 200 m of the cloud. This result led us to apply radiative cooling of cloud droplets to the upper portion of the cloud only [using Eq. (7) in section 2]. Tests were run with cooling applied to one grid point below cloud top (~100 m below cloud top, where cloud is defined by a cloud water mixing ratio >0.01 g kg^{-1}), and two grid points below cloud top (~200 m). The results showed differences less than 10% (see discussion later in this section), and thus we decided to apply cooling using Eq. (7) to only the first grid point below cloud top in the 2D model simulations. In addition, the droplet cooling rates predicted from the 1D detailed simulation and calculated with Eq. (7) were shown to be within 10% of each other, justifying the use of Eq. (7) to calculate the net radiative cooling of the droplets.

The results for the continental cloud with radiative cooling on (simulation 2) show that within 1 h the cloud

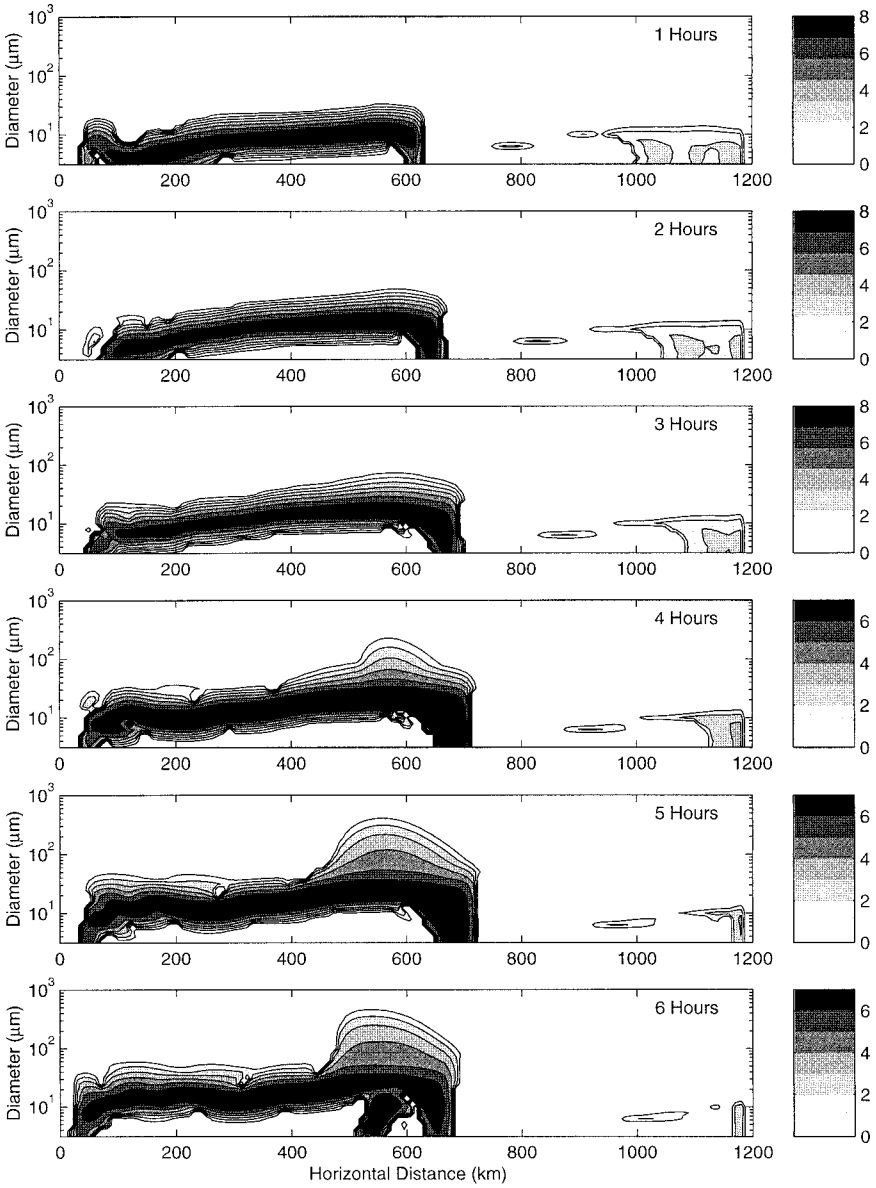

FIG. 8. Logarithmic gray shade contours of droplet number density [kg^{-1} (d logr^{-1})] using gray scale at the right as a function of water droplet diameter (vertical axis) and distance (km) 250 m above the ground level for simulation 1 (all warm continental simulation) at, from top to bottom: 1.0 h, 2.0 h, 3.0 h, 4.0 h, 5.0 h, and 6.0 h.

droplet size distribution becomes broader (Fig. 11) at cloud top (top panel). In fact, the distribution at cloud top becomes nearly identical with the maritime cloud droplet size distribution at the same time for simulation 7 in which radiative cooling is turned off (Fig. 10a), at least at times less than 2 h. The droplets from this distribution initiate the collision–coalescence process and the resulting drops fall through the cloud and form drizzle drops. This is evident in Fig. 11 by the progressive broadening of the spectra in time at all altitudes below cloud top. In contrast to the previous results, the formation of drizzle drops *does not occur at the same time at each altitude* (Fig. 11), but rather occurs later in time, the lower the altitude. This occurs due to the time required for the large drops initiated at cloud top to fall to lower levels in the cloud. The size distribution at the ground (bottom panel in Fig. 11) shows a tail forming in the distribution out to 200-μm diameter drops at 3 h. However, the number of drizzle drops formed is four orders of magnitude less in the continental case with radiative cooling than in the maritime case without the radiative term (cf. lower panels in Figs. 10a and 11). As a result, the maximum drizzle mixing ratio for this continental case with radiative cooling at 3 h is only

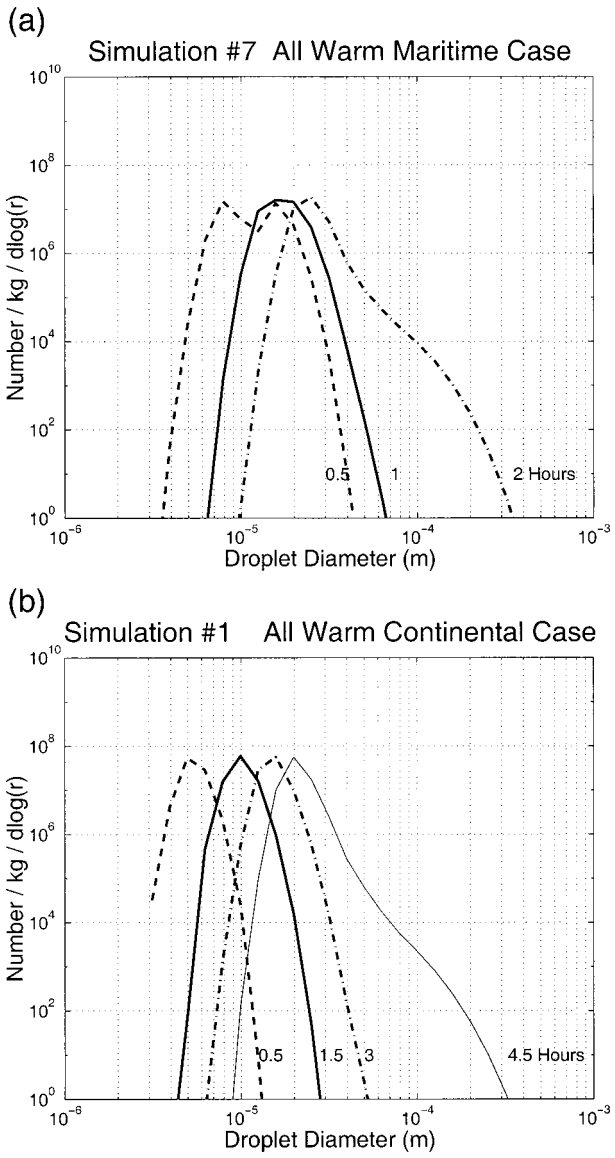

FIG. 9. Droplet size spectra 250 m AGL following a parcel of air: (a) spectra from simulation 7 (all warm maritime) starting 162 km upstream of the mountain top at $t = 0$, and ending at mountain top at $t = 3$ h. Spectra shown at 0.5 (135), 1.0 (108), and 2 (54) h (km), respectively, along the trajectory. (b) Spectra from simulation 1 (all warm continental) starting 324 km upstream of the mountain top at $t = 0$ and ending at mountain top at $t = 6$ h. Spectra shown at 0.5 (297), 1.5 (243), 3.0 (162), and 4.5 (81) h (km) along the trajectory.

0.00023 g kg^{-1}, nearly three orders of magnitude less than the maximum drizzle water simulated in the maritime case at the same time (0.105 g kg^{-1}). When the depth of radiative cooling near cloud top is doubled (simulation 11), the drizzle water mixing ratio at 3 h is only increased to 0.003 g kg^{-1}.

Since the maritime cloud has a broad size distribution throughout the cloud, large drops from air parcels at all levels can contribute to the observed drizzle water content in the cloud with the maritime CCN, while in the continental case with radiative cooling of drops near cloud top, only the drops formed near cloud top that fall through the cloud can contribute. As a result, the onset of freezing drizzle in the continental case with radiative cooling is similar to that of the continental case without radiative cooling (Fig. 12). The rate of drizzle formation is more rapid in the radiative cooling case, however, than the nonradiative cooling case. These results are similar to the results of Harrington et al. (2000) regarding the sensitivity of drizzle production to radiative cooling near the tops of arctic stratocumulus clouds. In our case the low drizzle amounts formed are due to the: 1) sedimentation of larger droplets from the cloud-top region where radiative cooling is active, limiting the build up of drizzle and 2) the limited number of drizzle embryos available to the cloud from the relatively small percentage of the cloud effected by radiative cooling. In the stratocumulus cloud, the minor effect of radiative cooling on drizzle formation is due to the short residence time of air parcels near cloud top, limiting the time available to broaden the distribution.

The maximum drizzle water content in the continental radiative cooling case prior to the normal onset of drizzle at 3 h was less than 0.01 g kg^{-1} (maximum at 3 h of 0.00023 g kg^{-1} compared to maximum of 0.000014 in the continental case with no radiative cooling at the same time). Aircraft observations of drizzle liquid water content (Fig. 18; Miller et al. 1998; Politovich 1989; Cober et al. 1996) show that nearly all observations of freezing drizzle conditions have water contents larger than 0.01 g m^{-3}, with the more hazardous drizzle conditions occurring for drizzle liquid water contents $> \sim 0.1$ g m^{-3}. Thus, the slight increase in drizzle water content due to cloud-top radiative cooling is not likely to result in hazardous drizzle conditions for aircraft. In fact, any mechanism for droplet spectral broadening near cloud top, such as the proposed shear mechanism (Pobanz et al. 1994), may only produce limited amounts of drizzle in clouds with weak updrafts according to these simulations due to the relatively small region in which the cloud droplet spectrum is broadened as compared to the entire cloud depth and the rapid sedimentation of the larger droplets. In the maritime CCN simulations, the size distribution is broadened throughout the entire cloud depth, allowing large drops to contribute from a number of different levels, leading to the higher drizzle water contents in these types of clouds.

Radiative cooling of cloud droplets may be responsible for drizzle formation in thin clouds with continental CCN. In these types of cloud, radiative cooling may be the only mechanism capable of broadening the size distribution to large enough sizes to initiate the collision–coalescence process. The drizzle water content of the clouds would be quite low, however. Harrington et al. (2000) showed that thin stratocumulus clouds ($<$500 m thick) with continental CCN only produced small amounts of drizzle. Radiative cooling may also be responsible for the formation of drizzle in clouds

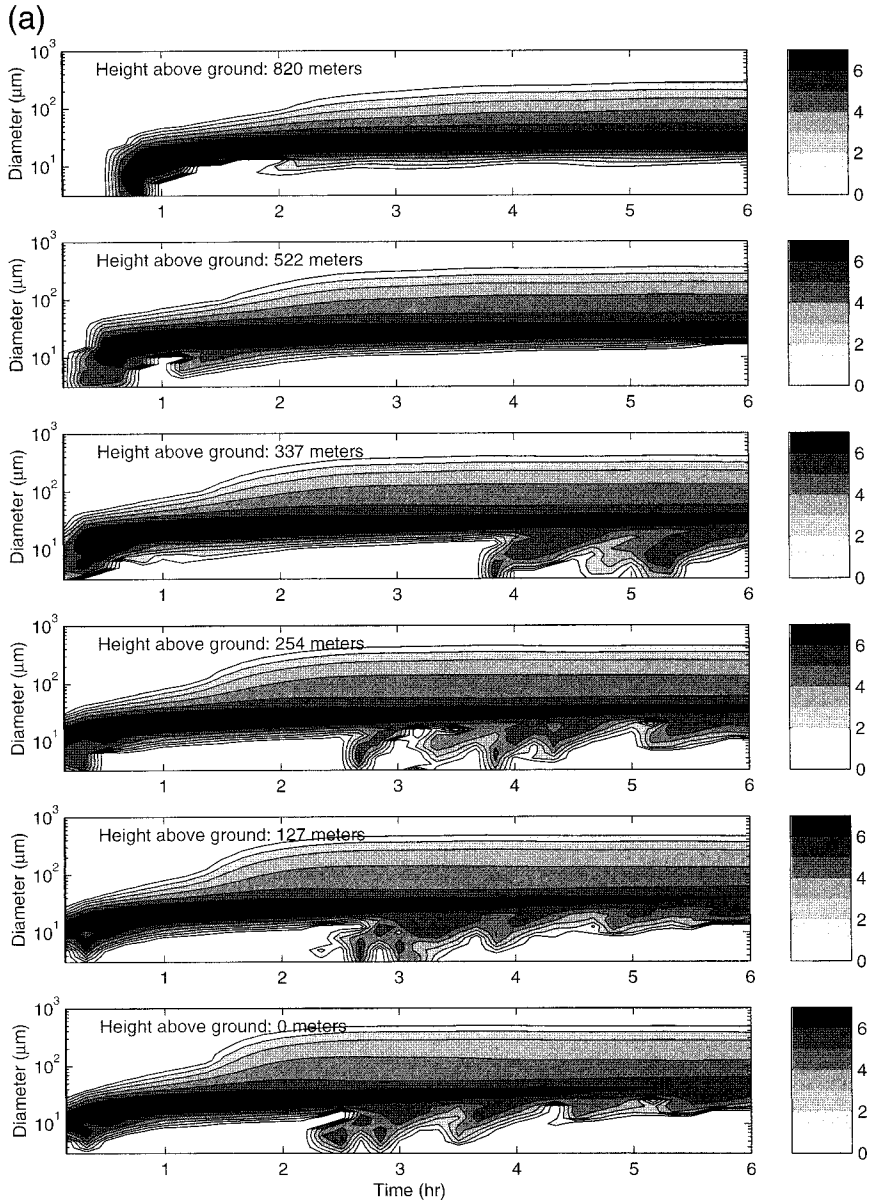

FIG. 10. Logarithmic gray shade contours of droplet number density [kg^{-1} $(d \log r)^{-1}$] using gray scale at the right as a function of water droplet diameter (vertical axis) and time of simulation at a distance 50 km upstream of the mountain peak for: (a) simulation 7 (all warm maritime simulation), and (b) simulation 1 (all warm continental simulation). In each figure the individual panels are for altitudes above ground level of, from top to bottom: 820, 522, 337, 254, 127, and 0 m as indicated.

with weak updrafts (<5 cm s^{-1}) and low liquid water contents.

In the simulation with a maritime CCN distribution and cloud droplet radiative cooling near cloud top (simulation 8), the cloud droplet distribution near cloud top is broadened even further. However, the maximum drizzle water content achieved by this simulation was not significantly increased over the simulation performed with no radiative cooling of cloud droplets (Fig. 12). This is consistent with the discussion above in that only affecting the cloud-top region will not significantly impact the drizzle forming capability of the cloud.

d. Sensitivity of freezing drizzle formation to ice initiation

To examine the effect of ice initiation on freezing drizzle formation, we performed simulations 5 (Meyers ice initiation) and 6 (Cooper ice initiation). Both of these simulations used a maritime CCN distribution and had

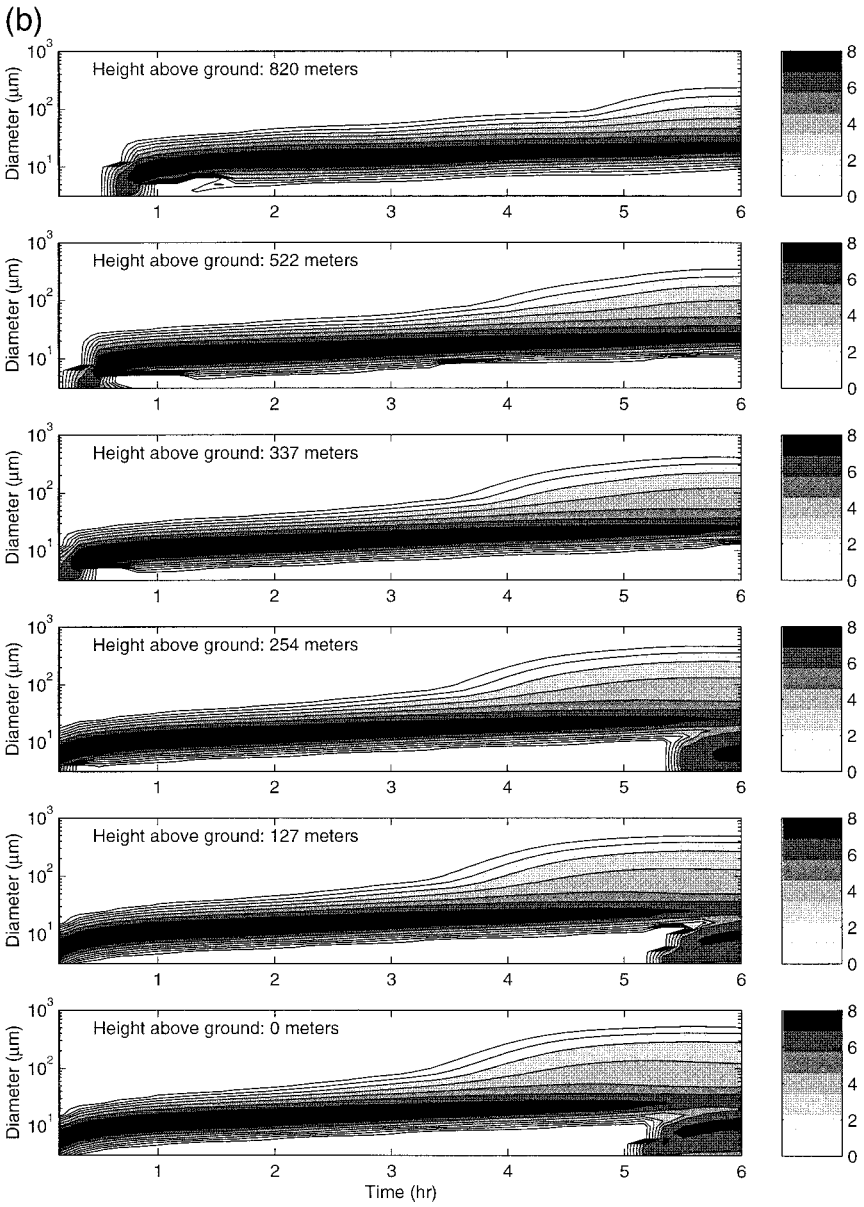

FIG. 10. (*Continued*)

radiative cooling of drops turned on. The main feature of simulation 6 was the relatively low ice-crystal concentrations produced by the Cooper method of ice initiation (0.08 L^{-1} maximum, see Fig. 2). In contrast, the simulation using the Meyers curve (simulation 5) formed nearly an order of magnitude more ice at these high temperatures (0.6 L^{-1} maximum, see Fig. 2), leading to enhanced formation of rimed ice crystals, aggregates, and graupel. As a result, the maximum cloud water is only 0.26 g kg^{-1} at 3 h in the Meyers simulation (Fig. 13). The maximum rainwater content at 3 h is a factor of two less than in the Cooper case and forms over a much more limited area near the top of the barrier (Fig. 14). The factor of 10 higher ice concentration in the Meyers case leads to increased depletion of cloud water by the riming of pristine ice crystals into rimed crystals and further riming of the rimed crystals and also by depositional growth. In both the Cooper and Meyers cases, riming and depositional growth of pristine ice and rimed ice contributes nearly equally to the increase in ice mass. However, the water vapor deposited on the ice particles in the Meyers case is an order of magnitude greater than in the Cooper case, as well as the riming.

The riming process depletes the larger droplets more than the smaller droplets due to the higher collision

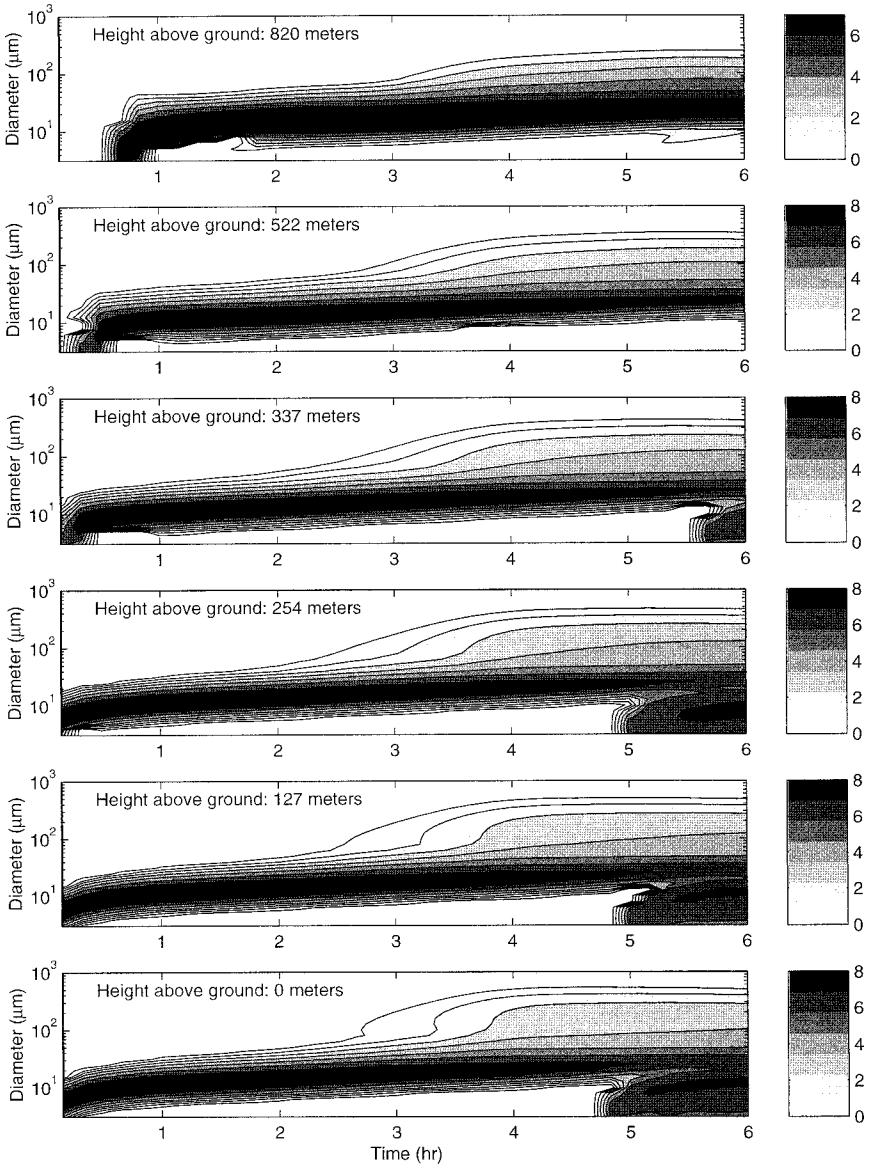

FIG. 11. Logarithmic gray shade contours of droplet number density [kg^{-1} (d log$r$)$^{-1}$] using gray scale at the right as a function of water droplet diameter (vertical axis) and time of simulation at a distance 50 km upstream of the mountain peak for simulation 2 (all warm continental simulation with radiative cooling of drops on). The various panels are for altitudes above ground level of, from top to bottom: 820, 522, 337, 254, 127, and 0 m as indicated.

efficiency between ice crystals and large droplets as compared to smaller droplets. Thus, higher ice-crystal concentrations will result in a rapid depletion of large cloud droplets. The reduced cloud water and numbers of larger droplets, in turn, leads to less conversion of cloud water to rainwater via the collision–coalescence process. As a result, the precipitation at the ground for the Meyers simulation (Fig. 15a) is mainly composed of rimed crystals as opposed to freezing drizzle, while in the Cooper case (Fig. 15b) most of the precipitation at the ground is freezing drizzle, with rimed crystal mass a factor of 3 less than in the Meyers case. Thus, a significant fraction of the cloud water and vapor in the Meyers case is converted to rimed crystals instead of drizzle.

In the liquid-only simulation 8, the cloud water mixing ratio reaches a value of 0.40 g kg^{-1} at 3 h, nearly the same value of the cloud water mixing ratio from simulation 6 (Cooper ice initiation) at the same time (0.39 g kg^{-1}). As a result, the maximum drizzle water content is nearly the same for both cases (0.105 g kg^{-1} for the no ice case, 0.09 g kg^{-1} for the Cooper case),

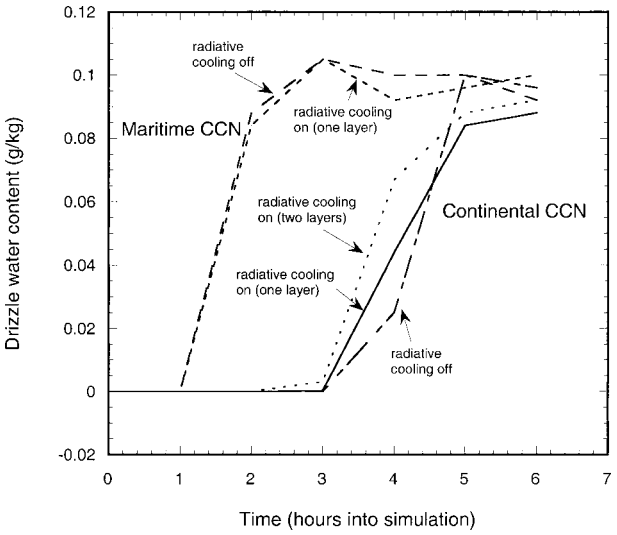

FIG. 12. Time series of maximum drizzle water content for the all warm maritime simulations with radiative cooling of drops on (simulation 8) and off (simulation 7) and for the all warm continental simulations with radiative cooling of drops on for one grid point below cloud top (simulation 2), radiative cooling for two grid points below cloud top (simulation 11) and no radiative cooling (simulation 1).

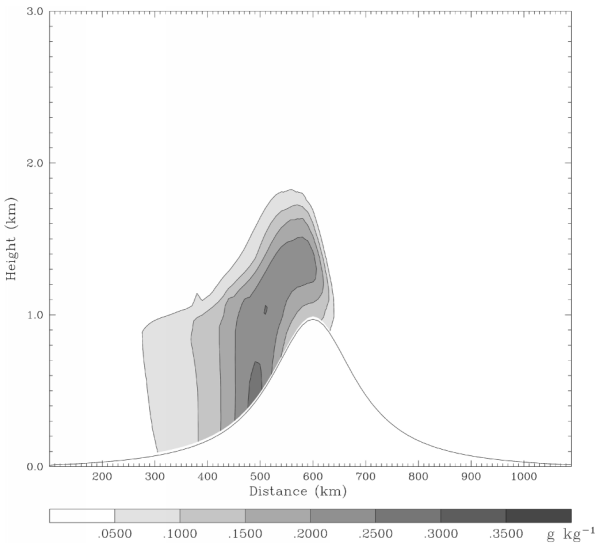

FIG. 13. Two-dimensional vertical cross section of cloud water mixing ratio (g kg^{-1}) from maritime simulation with Meyers ice (simulation 5) at 3 h. Grayscale values and units indicated in the legend on the bottom of each panel.

suggesting that the Cooper ice initiation scheme has minimal effect on the formation of freezing drizzle as compared to the liquid-only simulation, at least in the case of maritime CCN tested here.

While the difference in drizzle formation between the all warm maritime CCN case and the maritime simulation with Cooper ice was relatively small, in the continental simulations it was more significant. The maximum drizzle water was reduced by 30% in a simulation with continental CCN and Cooper ice (simulation 12) as compared to the maritime simulation with Cooper ice (simulation 6). The effect seems to be due to a reduction in overall cloud water and the larger drops by the riming of crystals, leading to a less efficient collision coalescence process. Thus, the presence of ice is shown to further inhibit the formation of drizzle in continental clouds.

The results in this section show that the formation of freezing drizzle is very sensitive to the number of ice crystals initiated. Note that the ice-crystal concentrations predicted from the Meyers and Cooper ice initiation schemes have the largest difference at -5°C (two orders of magnitude), decreasing to a factor of 50 difference at -10°C. This is the most common temperature range in which freezing drizzle is observed to form. The Meyers scheme has been successfully used in previous simulations of ice formation. The Cooper curve represents a fit to ice-crystal observations. The difference between these two schemes represents some of the natural variations in ice initiation observed in the atmosphere. In the case of freezing drizzle, the scheme with the smaller numbers of ice crystals initiated seems to produce more reasonable results. In other cases the Cooper scheme may underestimate ice formation. The current results highlight the strong sensitivity of freezing drizzle formation to ice initiation. Recent studies by Jiang et al. (2000), Harrington et al. (1999), and Pinto (1998) have all shown that the dynamics of arctic stratocumulus clouds are also strongly sensitive to the method of ice initiation used. More research is clearly needed on ice initiation before it can be properly simulated in models.

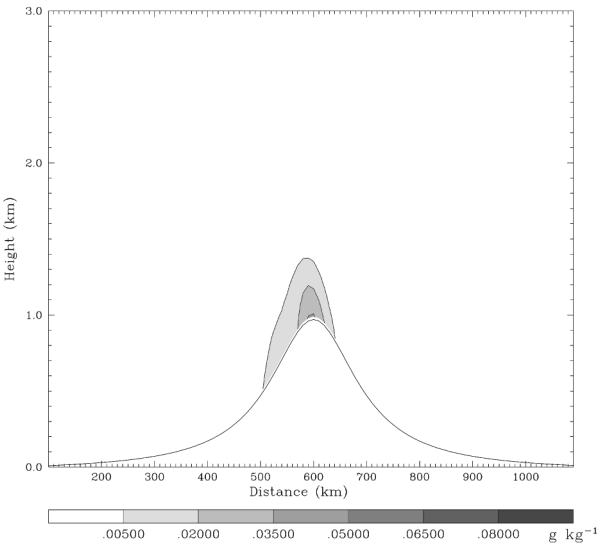

FIG. 14. Two-dimensional vertical cross section of drizzle water mixing ratio (g kg^{-1}) from the maritime simulation with Meyers ice (simulation 5) at 3 h. Grayscale values and units indicated in the legend on the bottom of each panel.

(a)

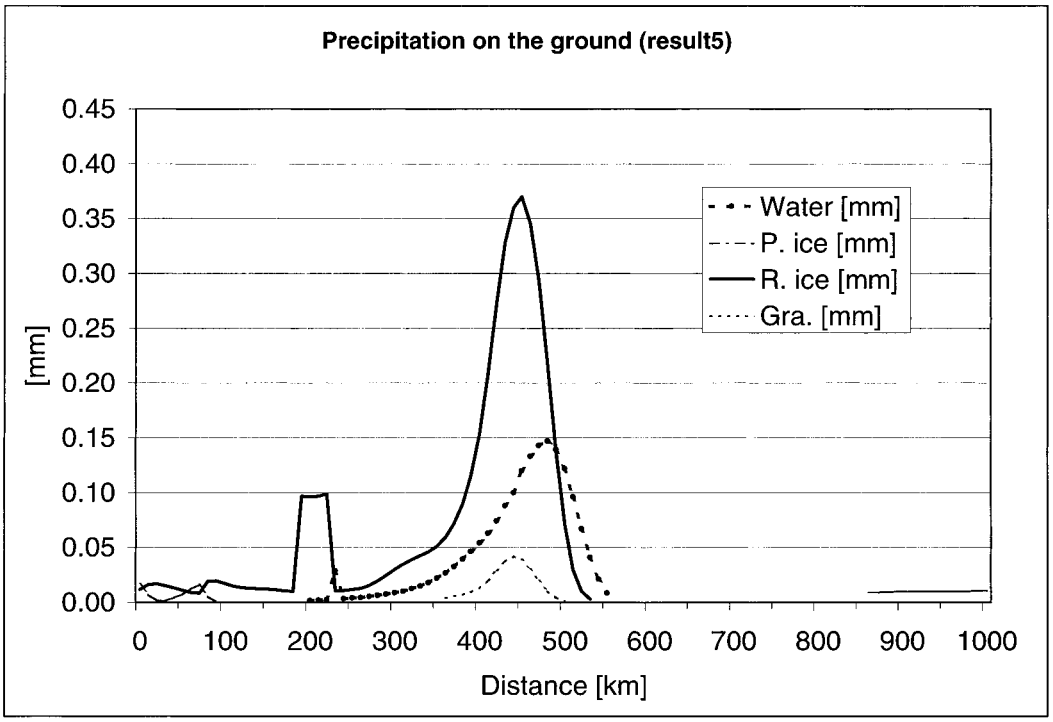

(b)

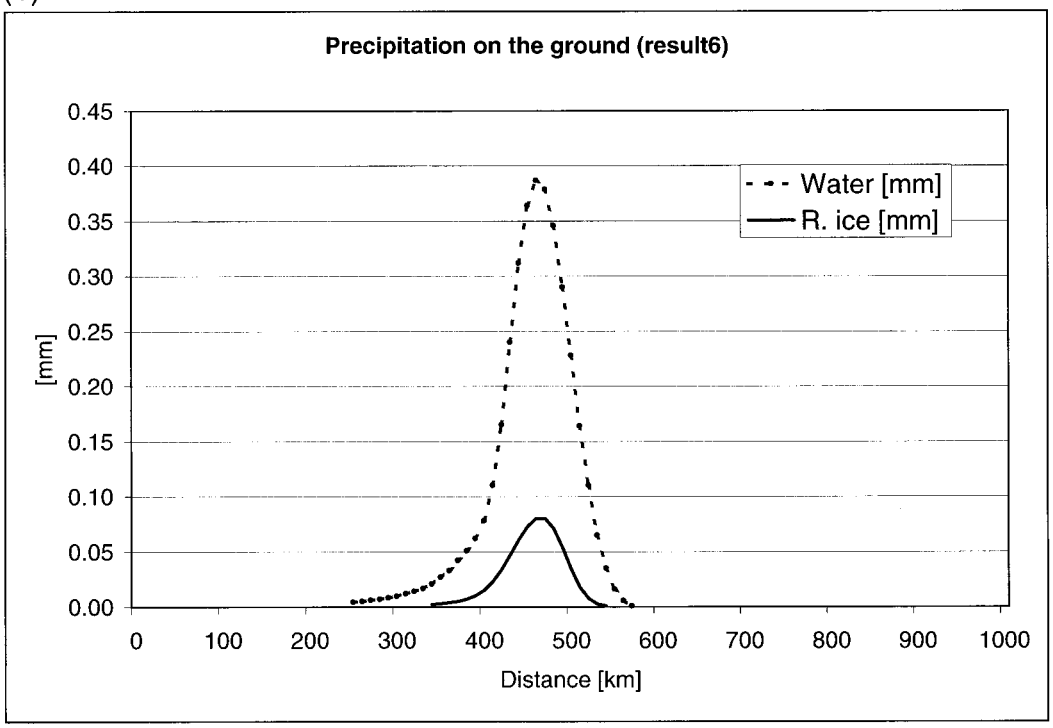

FIG. 15. Precipitation on the ground in millimeters at 3 h for the various hydrometeor types in: (a) Meyers ice initiation (simulation 5) and (b) Cooper ice initiation (simulation 6).

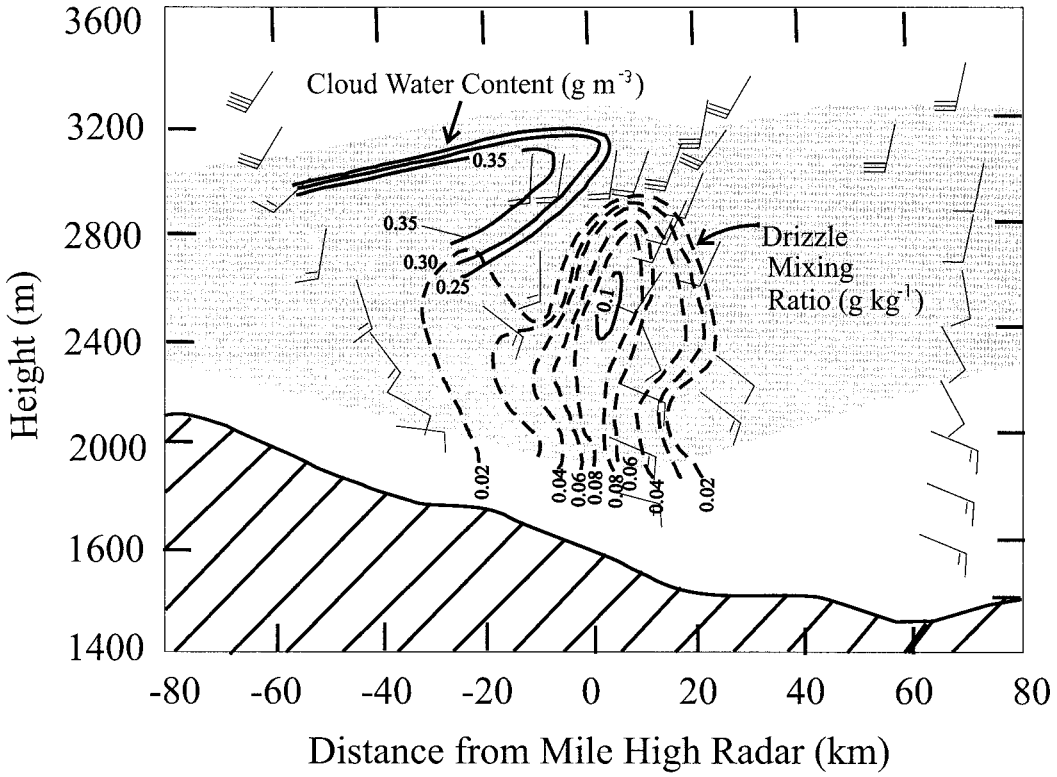

FIG. 16. North–south two-dimensional cross section of cloud water content (g m^{-3}) and drizzle water mixing ratio (g kg^{-1}) from aircraft data collected during the 1990 Valentine's Day freezing drizzle event in Colorado (Rasmussen et al. 1995). Locations of wind barbs indicate the aircraft track and location of data used to construct the cross section. Full barb represents 5 m s^{-1} and half-barb 2.5 m s^{-1}. Minimum cloud water contour plotted is 0.25 g m^{-3}. The light gray shading indicates the cloud layer. Hatched region indicates topography. Distance is given in kilometers north (positive numbers) and south (negative numbers) of the location of Mile High Radar. Location of Mile High Radar is approximately 18 km northeast of Denver. For further details regarding the aircraft data used to construct this cross section, see Rasmussen et al. (1995).

e. Sensitivity to ice nuclei depletion

In this section we compare simulations 6 and 10 with ice nuclei depletion on and off. In simulation 6, freezing drizzle starts to form after 1 h of simulation time and reaches a maximum mixing ratio of 0.084 g kg^{-1} after 3 h of simulation time (Fig. 5b). In simulation 10 without ice nuclei depletion, no drizzle forms even after 3 h. This is due to the significantly higher numbers of ice crystals nucleated in this case compared to the ice nuclei depletion case. These crystals rapidly deplete the available water and prevent the formation of drizzle. The scheme without ice nuclei depletion initiates new ice crystals whenever the current ice-crystal concentration falls below the Cooper or Meyers scheme estimate of the maximum number of ice crystals possible. Thus, when pristine ice crystals fall out, new ice is initiated to take their place. In the scheme with ice nuclei depletion, no ice crystals are nucleated since the sedimenting pristine ice crystals depleted the ice nuclei in the volume. Thus, the proper simulation of freezing drizzle in the case of weak updrafts *requires* that ice nuclei be depleted!

5. Comparison to observations

a. Comparison to the Valentine's Day freezing drizzle event in Colorado

The above-described model runs were designed to simulate observed occurrences of freezing drizzle formation. In particular, the height and width of the 2D mountain were designed to simulate the observed extent and magnitude of the updraft field observed during the 1990 Valentine's Day freezing drizzle event in Colorado (Rasmussen et al. 1995). In that case, the updraft magnitude was from 4 to 8 cm s^{-1} over a depth of approximately 1 km and a horizontal scale of a 100 km as determined from radar VAD profiles and aircraft data. Figure 16 shows the observed north–south vertical cross section of cloud water and drizzle water content from that case based on the aircraft data. As shown, the peak cloud water content reached is 0.35 g m^{-3}, or 0.35 g kg^{-1} based on the air density in this case having a value close to 1.0 kg m^{-3}. This value agrees very well with the observed near-steady-state maximum cloud water mixing ratio in the current maritime CCN simulations

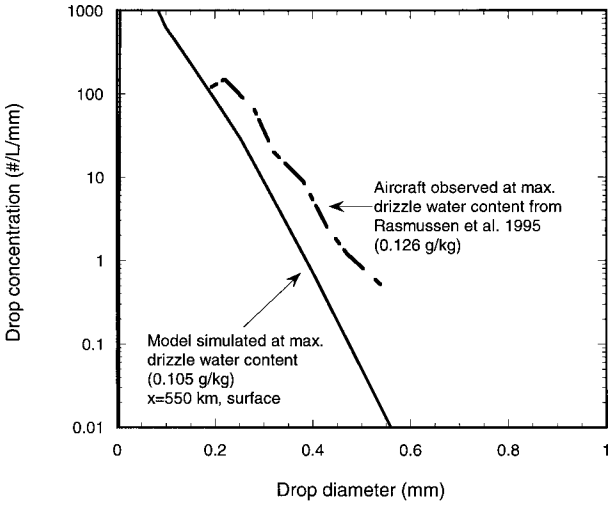

FIG. 17. Drizzle droplet spectra at maximum drizzle mixing ratio from model simulation 7 (all warm maritime simulation) and from the Valentine's Day freezing drizzle case (see previous figure for location of drizzle maximum in the observations). Observed drizzle spectra determined from 2D-C PMS probe for droplets greater than 150 μm.

between 0.36 and 0.44 g kg^{-1} (Fig. 6). The tilt of the cloud water region toward the north (the right in the figure) in the observations is also evident in the model results, with a similar slope of 0.2 km in the vertical for a horizontal distance change of 50 km. Freezing drizzle is observed to form just below and slightly downstream of this maximum of cloud water in both the observations and in the simulations. The drizzle mixing ratio in the observations (Fig. 16) reaches maximum values of 0.12 g kg^{-1}, in good agreement with the maximum values reached in the maritime CCN simulations (0.105 g kg^{-1} maximum). The observed drizzle size distribution near the maximum drizzle water content is compared to the model drizzle size distribution at maximum drizzle water content in Fig. 17. The agreement is very good, with both the model and aircraft observed spectra being approximately exponential with similar slope and y intercept. Since we are using a detailed microphysical model, the simulated size distribution is not constrained to be exponential in this case as in many bulk microphysical models.

Another important comparison between the current simulations and Valentine's Day case observations is for the ice-crystal concentrations. In the Valentine's Day case, ice crystal concentrations (mainly heavily rimed crystals or graupel) in the freezing drizzle region ranged from 0.01 to 0.09 L^{-1}, with a value of 0.05 L^{-1} at the location of maximum drizzle water content. This compares well with the ice-crystal concentrations in the simulations with the Cooper initiation scheme (range between 0.01 to 0.08 L^{-1}, 0.08 L^{-1} at the location of the drizzle water maximum).

Rasmussen et al. (1995) suggested that either low CCN concentrations or a cloud-top mixing process could be responsible for the formation of freezing drizzle in the Valentine's Day event. The current results suggest that the most likely factor leading to freezing drizzle in that case was low concentrations of CCN, consistent with the observed low concentrations of cloud droplets (50 cm^{-3}) and the difficulty in producing significant amounts of freezing drizzle via a cloud-top mixing process.

b. Comparison to a maritime freezing drizzle case

Cober et al. (1996) present aircraft observations of drizzle formation in an 1100-m deep stratiform cloud with -12°C cloud top over the ocean in which they identify the collision–coalescence process as the primary mechanism for drizzle formation. Vertical motion estimated for this cloud was 5–7 cm s^{-1}, and ice-crystal concentration in the region of drizzle was estimated to be 0.08 L^{-1} for particles larger than 0.5-mm diameter. Maximum drizzle water content measured was 0.07 g kg^{-1}, and maximum cloud water content was 0.2 g kg^{-1}. The air mass was determined to be quite clean with low cloud droplet concentrations of 24 cm^{-3}. The above-described conditions (vertical motion, cloud thickness, and cloud-top temperature) are very similar to those simulated in this study. The microphysical conditions (low CCN, low ice-crystal concentrations) are similar to simulation 6, which was the maritime CCN case with Cooper ice initiation. The predicted drizzle water content is of similar magnitude to the Cober case (0.1 g kg^{-1} predicted, 0.07 g kg^{-1} observed), while the cloud water content measured is less (0.36 g kg^{-1} predicted, 0.2 g kg^{-1} observed). The latter difference may be due to the lower CCN in the observed case as compared to the current simulation, requiring less liquid water for the onset of the collision–coalescence process, as found in the current and previous studies (e.g., Feingold et al. 1996).

Of particular interest are the low ice-crystal concentrations observed in the Cober et al. case. The observed ice-crystal concentration in the region of freezing drizzle was 0.08 L^{-1} for particles larger than 0.5 mm, while the model-predicted maximum ice-crystal concentration at the location of maximum drizzle was 0.076 L^{-1} (simulation 6) for particles of this size. The agreement between the model and observations is quite good in this case. Cober et al. (1996) observed a lack of drizzle in a nearby region with colder cloud-top temperatures and higher ice-crystal concentrations of 0.2 L^{-1} for crystals larger then 0.5 mm. The simulation with the Meyers ice initiation scheme (simulation 5), in which freezing drizzle formation was suppressed due to high ice-crystal concentrations, had ice-crystal concentrations very similar to those observed in this nearby region by Cober et al. (0.36 L^{-1} for crystals greater than 0.5 mm at the location of maximum drizzle). This scenario was also observed in the Valentine's Day case studied by Rasmussen et al. (1995) in the northern portion of the strat-

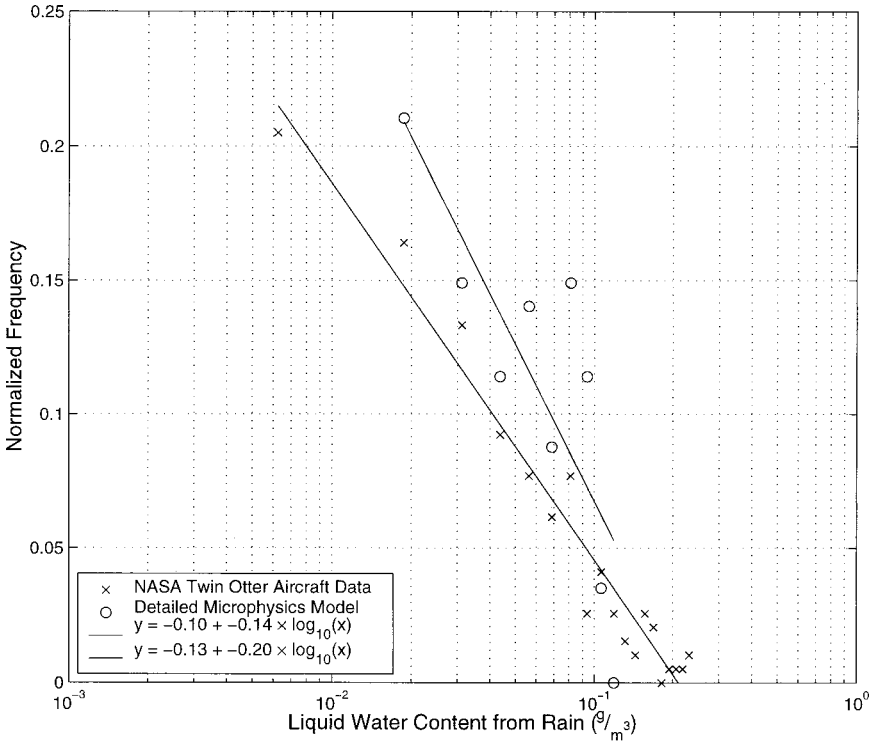

FIG. 18. Normalized frequency of occurrence of drizzle water content from National Aeronautics and Space Administration Twin Otter aircraft measurements in drizzle clouds (X's) compared to drizzle water contents derived from drizzle regions from the all warm maritime simulation (7) at 3 h (open circles). Drizzle drops are defined as drops larger than 50 μm diameters.

iform cloud, where colder cloud tops, higher ice-crystal concentrations and no drizzle was observed. Thus, the strong sensitivity of freezing drizzle formation to ice-crystal concentration is noted both in the observations and in the current model simulations.

c. Comparison to observed drizzle water contents

Drizzle water contents from a number of field programs are compared to model drizzle water contents from the maritime simulation 7 in Fig. 18. The drizzle water contents were obtained from data collected by the NASA/Glenn instrumented Twin Otter in drizzle events in the southern Great Lakes region (Miller et al. 1998). Drizzle water contents in both the observations and model simulations are for droplet diameters greater than 50 μm. The frequency of occurrence of various liquid water contents is given. As shown, both the observations and simulations show an exponential dependence of frequency of occurrence of drizzle water content, with similar slope and *y* intercept. Observed drizzle water contents range between 0.006 and 0.25 g m^{-3}. The above agreement gives additional confidence that the model simulation of freezing drizzle through a collision–coalescence process is similar to that occurring in nature.

6. Summary and conclusions

This study has investigated various mechanisms for freezing drizzle formation by performing simulations of stably stratified cloud formation over a bell-shaped mountain using a detailed microphysical model embedded in the MM5 mesoscale model. A comparison to observations showed that the simulations were able to replicate key features of observed freezing drizzle formation. The results of the simulations show:

1) *Low CCN concentrations leads to rapid formation of freezing drizzle.*

   This occurs due to the broad cloud droplet size distribution formed throughout the cloud in this case, allowing for rapid broadening of the spectra to the point at which the collision–coalescence process is initiated. This mechanism starts to produce drizzle after 1 h of simulation time in mesoscale updrafts of 4–10 cm s^{-1}. Since the air mass involved in frontal lifting is often above the atmospheric boundary layer, and CCN concentrations are usually significantly lower above the boundary layer (Pruppacher and Klett 1997), the occurrence of low CCN in these types of clouds is not unexpected. Lower ice-crystal concentrations are also observed above the boundary layer (Rasmussen et al. 1995), and thus these types

of frontal clouds may be preferred regions for freezing drizzle formation due to the presence of low CCN and low ice-crystal concentrations. These results also confirm previous hypotheses by Murakami (1992), Rasmussen et al. (1995), and Cober et al. (1996) based on observations that low concentration of CCN is one of the primary mechanisms for drizzle production.

2) *Continental clouds can produce freezing drizzle given sufficient depth and time.*

   The current results suggest that stably stratified clouds with continental CCN *can* form freezing drizzle if the mesoscale updraft and warm cloud-top conditions can be maintained for periods greater than 4 h. It also suggests that the region of mesoscale updraft must be sufficiently broad and steady state to support 4 h of uplift.

3) *Radiative cooling of the cloud droplets near cloud top can be effective in broadening an initially continental droplet spectrum toward that of a maritime cloud droplet size distribution.*

   Maximum drizzle water mixing ratios produced by this mechanism were 2.0×10^{-4} g kg^{-1}. The lowest drizzle mixing ratios observed with instrumented aircraft are on the order of 0.005 g kg^{-1} (Politovich 1989; Cober et al. 1996), thus the radiative cooling of drops mechanism may not act over a sufficiently deep volume of the cloud to produce observed freezing drizzle mixing ratios. It can, however, produce low concentrations of freezing drizzle over a broad region, and may help account for the formation of low concentrations of drizzle in thin clouds and clouds with weak updrafts and low water content.

4) *Any mechanism that only broadens the cloud droplet spectra near cloud top (such as radiative cooling or a cloud top mixing process) may not act over a sufficiently broad volume of the cloud to produce significant amounts of freezing drizzle.*

   The current results suggest that the mechanism for cloud droplet spectral broadening needs to operate throughout the volume of the cloud in order to produce the observed drizzle mixing ratios as well as the higher drizzle mixing ratios known to be hazardous to aircraft in flight.

5) *Freezing drizzle formation is very sensitive to ice initiation.*

   Low ice-crystal concentrations (<0.08 L^{-1}) in the region of freezing drizzle formation were found to be a necessary condition for drizzle formation (from both model and observations). Drizzle formation in high CCN clouds was significantly reduced due to the presence of ice, while low CCN clouds were relatively unaffected.

6) *The formation of freezing drizzle in the model required the depletion of ice nuclei.*

   If ice nuclei were not depleted, ice-crystal concentrations built up to unrealistic levels due to the initiation of new ice crystals after the ice crystals in the volume fell out. No freezing drizzle formed in simulations without ice nuclei depletion for either the Meyers or Cooper scheme.

7) *The maximum cloud water mixing ratio and threshold amount for the onset of drizzle in stably stratified clouds was shown to depend strongly on the CCN concentration.*

8) *A key factor controlling the formation of freezing drizzle in stratified clouds is the lifetime of the mesoscale and synoptic conditions and the thickness and length of the cloud.*

   If a stratiform cloud with a thickness greater than 800 m, length longer than $V_{\text{mean}} \times 4.5$ h, saturated updrafts on the order of 5–20 cm s^{-1}, and cloud-top temperatures greater than -12°C, can be maintained for longer than 4.5 h, then freezing drizzle will occur independent of CCN distribution, cloud-top mixing, and wind shear. The V_{mean} is the mean velocity in the cloud layer. Low CNN concentration reduces the time needed for drizzle to form down to 2 h, the thickness of the cloud down to as little as 200 m, and the length of the cloud to $V_{\text{mean}} \times 2$ h or 2.25 times shorter than the equivalent continental cloud to form drizzle. A schematic diagram comparing the minimum cloud size for a continental drizzle cloud to the minimum maritime drizzle cloud size is given in Fig. 19. As shown, the minimum size for a maritime cloud to form drizzle is significantly smaller than for a continental cloud. Since smaller clouds of short duration occur more frequently than larger clouds of long duration, freezing drizzle is much more likely to form under low CCN conditions than under continental CCN conditions.

Thus, freezing drizzle forms when the appropriate mesoscale conditions (weak vertical velocities on the order of 5–10 cm s^{-1}), cloud conditions (stably stratified cloud with cloud-top temperatures greater than -12°C, no ice-crystal seeding from aloft, thickness of cloud greater than 200 m, and length greater than $V_{\text{mean}} \times 2$ h for maritime cloud, thickness greater than 800 m and length greater than $V_{\text{mean}} \times 4.5$ h for continental cloud), and microphysical conditions (low ice-crystal concentrations, typically less than 0.08 L^{-1}) last for a sufficiently long periods of time (2 h for low CCN conditions, 4.5 h for high CCN conditions). Previous observational studies of freezing drizzle are consistent with this scenario (Murakami et al. 1992; Rasmussen et al. 1995; Cober et al. 1996) as well as climatological studies of freezing drizzle (Bernstein 2000). Of particular relevance is the maritime or low CCN conditions found to favor freezing drizzle formation in all of the above studies. Thus, clean air masses favor drizzle formation due to the presence of low CCN and ice nuclei concentrations.

Acknowledgments. The authors are grateful to Marcia Politovich for providing the the drizzle water data from

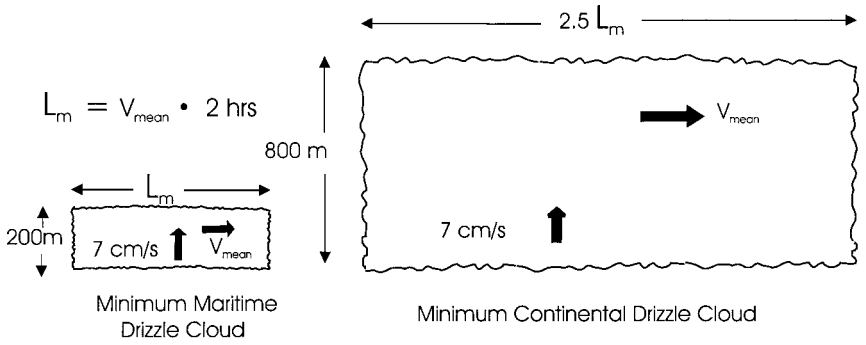

FIG. 19. Schematic of the minimum cloud size for drizzle formation. Depth and length of the cloud is annotated. Here V_{mean} is the mean airflow in the cloud, while L_m is the length of the maritime cloud. Also indicated is the vertical velocity assumed (7 cm s^{-1}).

the NASA/Glenn project. The authors also appreciate the helpful discussions with Ben Bernstein and Marcia Politovich on observations of freezing drizzle and their reviews of early versions of this manuscript. Constructive reviews by Graham Feingold and two anonymous reviewers significantly improved this manuscript. This research is in response to requirements and funding by the Federal Aviation Administration (FAA). The view expressed are those of the authors and do not necessarily represent the official policy of the FAA. This research was also supported by the Hungarian Research Fund (T30857).

APPENDIX

Specifics of the Detailed Microphysical Model

a. Description of the five different types of hydrometeors

Five different types of particles are involved in the model: water drops, pristine ice, rimed ice, aggregates, and graupel. The interactions between these five different types of hydrometeors are treated as in Reisin et al. (1996).

1) WATER DROPS

The terminal velocities of the water drops are calculated using the Best and Bond number approach as described in Pruppacher and Klett (1997). The collision efficiencies for drop–drop collision was calculated from the tabulated data of Hall (1980).

2) PRISTINE CRYSTALS

The pristine ice crystals are assumed to have the form of a thin hexagonal plate. When the diffusional growth of the pristine crystals is calculated, this shape is approximated by an oblate spheroid with two different axes. The density of the pristine ice crystals is 900 kg m^{-3}. The diameter of the crystals depends on the square root of the mass following Hobbs (1974):

$$d_{ic} = 16.28\sqrt{m_{ic}}.$$

The mass and the diameter are given in kg and m, respectively.

Terminal velocity of the pristine ice crystals is a linear function of the their diameter (Hobbs 1974):

$$v_{ic} = 304 d_{ic}\left(\frac{1.2}{\rho_a}\right)^{0.5},$$

where ρ_a is the density of the air. Collision efficiency of drop–pristine ice collision is given by parabolic functions fitted to the theoretically calculated data of Pitter (1977).

The aggregation of the pristine crystals forms aggregates. The collision efficiency is equal to zero if one of the colliding crystals is less then 20 μm and increases linearly to unity as the diameter of the crystal increases to 100 μm. The coalescence efficiency depends on the temperature using the following equation: $E_{coal,crystals} = \exp[0.38(T - T_o)]$ from Lin et al. (1983).

3) RIMED CRYSTALS

Riming of the hexagonal plate pristine ice crystals forms rimed ice crystals. The shape of the rimed ice crystals is also approximated as an oblate spheroid. Most of the water drops are collected at the edges of the crystals, increasing their axis ratio, while their mean density decreases during the riming. It is assumed that the axis ratio (r_{ric}) increases linearly with the crystal mass, while the mean density (ρ_{ric}) decreases linearly with the mass:

$$r_{ric} = \frac{c_{ric}}{a_{ric}} = a_1 m_{ric} + b_1 \qquad \rho_{ric} = a_2 m_{ric} + b_2,$$

where $a_1 = 655.63$ kg^{-1}, $b_1 = 0.08$ and $a_2 =$

$-409811.4463\ \mathrm{m}^{-3}$, $b_2 = 900\ \mathrm{kg\ m}^{-3}$. [$r_{\mathrm{ric}} = 0.08$ when the crystal mass is equal to $3.773\ 10^{-10}$ kg ($d_{\mathrm{ric}} \approx 100\ \mu$m) and $r_{\mathrm{ric}} = 0.5$ at the crystal mass of 1.089 g ($d_{\mathrm{ric}} \approx 19$ mm).] In this mass interval the density decreases from 900 to 450 kg m^{-3}.

The relation between the larger axis of the crystal and its mass is calculated in every bin:

$$d_{\mathrm{ric}} = \left(\frac{6}{\pi \overline{r}_{\mathrm{ric}} \overline{\rho}_{\mathrm{ric}}}\right)^{1/3} m_{\mathrm{ric}}^{1/3},$$

where r_{ric} and ρ_{ric} are calculated by the mean particle mass:

$$\overline{r}_{\mathrm{ric}} = a_1 \overline{m}_k + b_1 \qquad \overline{\rho}_{\mathrm{ric}} = a_2 \overline{m}_k + b_2,$$

where the mean mass (m_k) is the ratio of the mixing ratio (M_k) and the concentration (N_k) in the kth bin: $\overline{m}_k = M_k/N_k$. The terminal velocity of the rimed crystals is (Hobbs 1974):

$$v_{\mathrm{ric}} = \begin{cases} 1250 d (1.2/\rho_a)^{0.5} & \text{if } m < 5.654 \times 10^{-9}\ \mathrm{kg} \\ 4.84 d^{0.25} (1.2/\rho_a)^{0.5} & \text{if } m \geq 5.654 \times 10^{-9}\ \mathrm{kg}. \end{cases}$$

The collision efficiency of drop–rimed ice depends on the size of the drops and linearly increases from zero to unity as the diameter of the drop increases from 5 to 50 μm. The collision efficiency of rimed ice–rimed ice collision is equal to unity and the coalescence equation depends on the temperature using the following equation: $E_{\mathrm{coal,rimed}} = \exp[0.09(T - T_o)]$ from Lin et al. (1983).

4) AGGREGATES

Aggregates are formed by self-collection of the pristine and rimed ice crystals. The relationship between the density and the size and between the size and the terminal velocity are based on Passarelli and Srivastava (1979). The collision efficiency of the drop–aggregate collision depends only on the size of the drops. It is zero if the size of the drop is less then 5 μm and increases linearly to unity as the drop diameter increases to 20 μm.

5) GRAUPEL

Graupel particles are assumed to have spherical symmetry. Their density depends on the size, increasing linearly from 450 to 900 kg m^{-3} as its mass increases from 4.189×10^{-9} to 4.289×10^{-6} kg (from about 100 μm to 1 mm in diameter).

The terminal velocity of the graupel particles is given by Rasmussen and Heysmfield (1987). The collision efficiency of the drop–graupel collision is given by the formula suggested by Langmuir (1948).

b. *Diffusional growth of pristine and rimed ice crystals*

The diffusional growth rate of pristine and rimed ice crystals was calculated using the relationships given in Pruppacher and Klett (1997). The effect of radiative cooling was neglected but the gas kinetic effect was considered in the case of pristine ice, but neglected for rimed ice.

c. *Analytical solution for the simultaneous diffusional growth of drops and pristine and rimed ice crystals. (The effect of radiative cooling for drops is taken into consideration.)*

Relationships for the simultaneous diffusional growth of drops, pristine ice crystals, and rimed ice crystals are derived following Reisin et al. (1996) with an additional term included for the radiative cooling of drops. This treatment extends the Harrington et al. (2000) development by also including diffusional growth of pristine and rimed ice crystals.

The water vapor mixing ratio excess over water and ice saturation are defined by: $\Delta S_w(t) = q_v - q_{s,w}$ and $\Delta S_i(t) = q_v - q_{s,i}$, where q_v is the vapor mixing ratio, and $q_{s,w}$ and $q_{s,i}$ are the saturation mixing ratio over flat water and ice surface, respectively. The following two differential equations give the time derivative for water and ice supersaturation excess, where $\mathrm{QR1}_w$ and $\mathrm{QR2}_w$ involve the radiative cooling of drops.

$$\frac{\partial \Delta S_w(t)}{\partial t} + R_w \Delta S_w(t) + P_i \Delta S_i(t) + \mathrm{QR2}_w = 0$$

$$\frac{\partial \Delta S_i(t)}{\partial t} + R_i \Delta S_i(t) + P_w \Delta S_w(t) + \mathrm{QR1}_w = 0.$$

The solutions to the above two equations are given by the following equations:

$$\Delta S_w(t) = \Delta S_w(t_0) - \left(\frac{R_w \Delta S_w(t_0) + P_i \Delta S_i(t_0)}{R_w + R_i} + \frac{\mathrm{QR2}_w R_w + \mathrm{QR1}_w P_i}{(R_w + R_i)^2}\right)(1 - e^{-(R_w + R_i)t})$$

$$\Delta S_i(t) = \Delta S_i(t_0) - \left(\frac{R_i \Delta S_i(t_0) + P_w \Delta S_w(t_0)}{R_w + R_i} + \frac{\mathrm{QR2}_w P_w + \mathrm{QR1}_w R_i}{(R_w + R_i)^2}\right)(1 - e^{-(R_w + R_i)t}).$$

During one time step the supersaturation could change sign, in this case a smaller time step, Δt^*, needs to be used. This smaller time step can be calculated from the above equation by substituting 0 in the left side of the above equations:

$$\Delta t_w^* = \frac{-1}{R_w + R_i} \ln\left[1 - \frac{\Delta S_w(t_0)}{C_1}\right]$$

$$\Delta t_i^* = \frac{-1}{R_w + R_i} \ln\left[1 - \frac{\Delta S_i(t_0)}{C_2}\right].$$

The above time steps are calculated if the terms within the ln are greater than 0. The new time step will be [Δt^* = minimum (Δt_w^*, Δt_i^*, Δt)].

d. Collision with contact nuclei

The freezing of the supercooled drops could be initiated by collision with active contact nuclei. The collection of the nuclei by water drops may occur due to Brownian or phoretic transports or gravitational collection. In this parameterization the contact nuclei are assumed to be monodisperse with radius of 0.1 μm. The scavenging of these particles are effected by Brownian and phoretic transports (gravitational collection rate is not calculated). The collection rates are from the paper by Young (1974).

The rate of formation of frozen drops by contact nucleation is given by

$$\frac{dN_k}{dt} = f \left.\frac{dN_{\mathrm{IN,C}}}{dt}\right|_{k,\mathrm{Ph+Br}} \qquad \frac{dM_k}{dt} = \int_{m_k}^{m_{k+1}} m \frac{dN_k}{dt}\, dm,$$

where $(dN_{\mathrm{IN,C}}/dt)\,|_{k,\mathrm{Ph+Br}}$ gives the concentration of the ice-forming nuclei collected by the drops in k*th* bin in unit time and

$$f = [N_c(t) - N_c^1]/[N_{\mathrm{IN,C}}(t)],$$

where N_c^1 is the concentration of activated ice nuclei after the calculation of advection and diffusion at a given grid point at time *t.* New ice particles could form if $f > 0$. Here $N_{\mathrm{IN,C}}(t)$ is the concentration of the aerosol particles that could become contact nuclei. Drops with radii less than 25 μm that are frozen by contact nucleation are categorized as pristine ice crystals, while larger drops are converted into graupel particles.

REFERENCES

Austin, P. H., S. Siems, and Y. Wang, 1995: Constraints on droplet growth in radiatively cooled stratocumulus clouds. *J. Geophys. Res.,* **100,** 14 231–14 242.

Bernstein, B. C., 2000: Regional and local influences on freezing drizzle, freezing rain and ice pellet events. *Wea. Forecasting,* **15,** 485–508.

——, T. A. Omeron, F. McDonough, and M. K. Politovich, 1997: The relationship between aircraft icing and synoptic-scale weather conditions. *Wea. Forecasting,* **12,** 742–762.

——, ——, M. K. Politovich, and F. McDonough, 1998: Surface weather features associated with freezing precipitation and severe in-flight icing. *Atmos. Res.,* **46,** 57–73.

Caughey, S. J., and M. Kitchen, 1984: Simultaneous measurements of the turbulent and microphysical structure of nocturnal stratocumulus cloud. *Quart. J. Roy. Meteor. Soc.,* **110,** 13–34.

Celik, F., and J. D. Marwitz, 1999: Droplet spectra broadening by ripening process. Part I: Roles of curvature and salinity of cloud droplets. *J. Atmos. Sci.,* **56,** 3091–3105.

Chen, C., and W. R. Cotton, 1987: The physics of the marine stratocumulus-capped mixed layer. *J. Atmos. Sci.,* **44,** 2951–2977.

Cober, S. G., J. W. Strapp, and G. A. Isaac, 1996: An example of supercooled drizzle drops formed through a collision-coalescence process. *J. Appl. Meteor.,* **35,** 2250–2260.

Cooper, W. A., 1986: Ice initiation in natural clouds. *Precipitation Enhancement—A Scientific Challenge, Meteor. Monogr.,* No. 21, Amer. Meteor. Soc., 29–32.

——, 1989: Effects of variable growth histories on droplet size distributions. Part I: Theory. *J. Atmos. Sci.,* **46,** 1301–1311.

——, W. R. Sand, M. K. Politovich, and D. L. Veal, 1984: Effects of icing on performance of research aircraft. *J. Aircraft,* **21,** 708–715.

Dudhia, J., 1993: A non-hydrostatic version of the Penn State–NCAR Mesoscale Model: Validation tests and simulation of an Atlantic cyclone and cold front. *Mon. Wea. Rev.,* **121,** 1493–1513.

Feingold, G., S. M. Kreidenweis, B. Stevens, and W. R. Cotton, 1996: Numerical simulations of stratocumulus processing of cloud condensation nuclei through collision-coalescence. *J. Geophys. Res.,* **101,** 21 391–21 402.

——, W. R. Cotton, S. M. Kreidenweis, and J. T. Davis, 1999: The impact of Giant Cloud Condensation Nuclei on drizzle formation in stratocumulus: Implications for cloud radiative properties. *J. Atmos. Sci.,* **56,** 4100–4117.

Geresdi, I., 1998: Idealized simulation of the Colorado hailstorm case: Comparison of bulk and detailed microphysics. *Atmos. Res.,* **45,** 237–252.

Hall, W. D., 1980: A detailed microphysical model within a two-dimensional framework: Model description and preliminary results. *J. Atmos. Sci.,* **37,** 2486–2507.

Harrington, J. Y., T. Reisin, W. R. Cotton, and S. M. Kreidenweis, 1999: Cloud resolving simulations of Artic stratus. Part II: Transition-season clouds. *Atmos. Res.,* **51,** 45–75.

——, G. Feingold, and W. R. Cotton, 2000: Radiative impacts on the growth of a population of drops within simulated summertime arctic stratus. *J. Atmos. Sci.,* **57,** 766–785.

Hobbs, P. V., 1974: *Ice Physics.* Oxford Press, 837 pp.

Huffman, G. J., and G. A. Norman Jr., 1988: The supercooled warm rain process and specification of freezing precipitation. *Mon. Wea. Rev.,* **116,** 2172–2182.

Isaac, G. A., S. G. Cober, A. V. Korolev, J. W. Strapp, A. Tremblay, and D. Marcotte, 1999: Canadian Freezing Drizzle Experiment. 37th AIAA Aerospace Science Meeting and Exhibit, American Institute of Aeronautics and Astronautics Paper AIAA 99-0492, 10 pp.

Jiang, H., W. R. Cotton, J. O. Pinto, J. A. Curry, and M. J. Weissbluth, 2000: Cloud resolving simulations of mixed-phase Arctic stratus observed during BASE: Sensitivity to concentration of ice crystals and large-scale heat and moisture advection. *J. Atmos. Sci.,* **57,** 2105–2117.

Kajikawa, M., K. Sakurai, and K. Kikuchi, 1988: Characteristic features of supercooled raindrops in the midwinter season of Arctic Canada. *J. Meteor. Soc. Japan,* **62,** 393–398.

Korelev, A. V., 1995: The influence of supersaturation fluctuations on droplet size spectra formation. *J. Atmos. Sci.,* **52,** 3620–3634.

——, and G. A. Isaac, 2000: Drop growth due to high supersaturation caused by isobaric mixing. *J. Atmos. Sci.,* **57,** 1675–1685.

Langmuir, I., 1948: The production of rain by a chain-reaction in cumulus clouds at temperatures above freezing. *J. Meteor.,* **5,** 175–192.

Lin, Y. L., R. Farley, and H. D. Orville, 1983: Bulk parameterization

of the snow field in a cloud model. *J. Climate Appl. Meteor.*, **22,** 1065–1092.
Marwitz, J., M. Politovich, B. Bernstein, F. Ralph, P. Neiman, R. Ashenden, and J. Bresch, 1997: Meteorological conditions associated with the ATR72 aircraft accident near Roselawn, Indiana, on 31 October 1994. *Bull. Amer. Meteor. Soc.*, **78,** 41–52.
Meyers, M. P., P. J. DeMott, and W. R. Cotton, 1992: New primary ice-nucleation parameterization in an explicit cloud model. *J. Appl. Meteor.*, **31,** 708–721.
Miller, D., T. Ratvasky, B. Bernstein, F. M. McDonough, and J. W. Strapp, 1998: NASA/FAA/NCAR supercooled large droplet icing flight research: Summary of winter 96–97 flight operations. 36th AIAA Aerospace Sciences Meeting and Exhibit, American Institute of Aeronautics and Astronautics Paper AIAA 98-0557, 20 pp.
Murakami, M., Y. Yamada, T. Matsuo, H. Mizuno, and K. Morikawa, 1992: Microphysical structures of warm-frontal clouds. The 20 June 1987 case study. *J. Meteor. Soc. Japan*, **70,** 877–895.
Ohtake, 1963: Hemispheric investigation of warm rain by radiosonde data. *J. Appl. Meteor.*, **2,** 594–607.
Passarelli, R. E., and R. Srivastava, 1979: A new aspect of snowflake aggregation theory. *J. Atmos. Sci.*, **36,** 484–493.
Pike, W. S., 1995: Extreme warm frontal icing on 25 February 1994 causes an aircraft accident near Uttoxeter. *Meteor. Appl.*, **2,** 273–279.
Pinto, J. O., 1998: Autumnal mixed-phase cloudy boundary layers in the Arctic. *J. Atmos. Sci.*, **55,** 2016–2038.
Pitter, R. L., 1977: A reexamination of riming on thin ice plates. *J. Atmos. Sci.*, **34,** 684–685.
Pobanz, B. M., J. D. Marwitz, and M. K. Politovich, 1994: Conditions associated with large-drop regions. *J. Appl. Meteor.*, **33,** 1366–1372.
Politovich, M. K., 1989: Aircraft icing caused by large supercooled droplets. *J. Appl. Meteor.*, **28,** 856–868.
——, 1996: Response of a research aircraft to icing conditions and evaluation of icing severity indices. *J. Aircraft*, **33,** 291–297.
Pruppacher, H. R., and J. D. Klett, 1997: *Microphysics of Clouds and Precipitation.* Kluwer Academic Publishers, 945 pp.
Rasmussen, R. M., and A. J. Heymsfield, 1987: Melting and shedding of hail and graupel. Part I. Model physics. *J. Atmos. Sci.*, **44,** 2754–2763.
——, and Coauthors, 1992: Winter Icing and Storms Project (WISP). *Bull. Amer. Meteor. Soc.*, **73,** 951–974.
——, B. Bernstein, M. Murakami, G. Stossmeister, and B. Stankov, 1995: The 1990 Valentine's Day Arctic Outbreak. Part I: Mesoscale and microscale structure and evolution of a Colorado Front Range shallow upslope cloud. *J. Appl. Meteor.*, **34,** 1481–1511.
Reisin, T., Z. Levin, and S. Tzivion, 1996: Rain production in convective clouds as simulated in an axisymmetric model with detailed microphysics. Part I. Description of the model. *J. Atmos. Sci.*, **53,** 497–519.
Roach, W. T. R., 1976: On the effect of radiative exchange on the growth by condensation of a cloud or fog droplet. *Quart. J. Roy. Meteor. Soc.*, **102,** 361–372.
Sand, W. R., W. A. Cooper, M. K. Politovich, and D. L. Veal, 1984: Icing conditions encountered by a research aircraft. *J. Climate Appl. Meteor.*, **23,** 1427–1440.
Stuart, R. A., and G. A. Isaac, 1999: Freezing precipitation in Canada. *Atmos.–Ocean*, **37,** 87–102.
Tzivion, S., G. Feingold, and Z. Levin, 1987: An efficient numerical solution to the stochastic collection equation. *J. Atmos. Sci.*, **44,** 3139–3149.
——, T. Reisin, and Z. Levin, 1999: A numerical solution of the kinetic collection equation using high spectral grid resolution: A proposed reference. *J. Comput. Phys.*, **148,** 527–544.
Young, K. C., 1974: The role of contact nucleation in ice phase initiation in clouds. *J. Atmos. Sci.*, **31,** 768–776.